Vertical Structure of Kelvin Waves in the Indonesian Throughflow Exit Passages

KYLA DRUSHKA, JANET SPRINTALL, AND SARAH T. GILLE

Scripps Institution of Oceanography, La Jolla, California

IRSAN BRODJONEGORO

Bandung Institute of Technology, Bandung, Indonesia

(Manuscript received 5 October 2009, in final form 19 April 2010)

ABSTRACT

The subsurface structure of intraseasonal Kelvin waves in two Indonesian Throughflow (ITF) exit passages is observed and characterized using velocity and temperature data from the 2004–06 International Nusantara Stratification and Transport (INSTANT) project. Scatterometer winds are used to characterize forcing, and altimetric sea level anomaly (SLA) data are used to trace the pathways of Kelvin waves east from their generation region in the equatorial Indian Ocean to Sumatra, south along the Indonesian coast, and into the ITF region.

During the 3-yr INSTANT period, 40 intraseasonal Kelvin waves forced by winds over the central equatorial Indian Ocean caused strong transport anomalies in the ITF outflow passages. Of these events, 21 are classed as ''downwelling'' Kelvin waves, forced by westerly winds and linked to depressions in the thermocline and warm temperature anomalies in the ITF outflow passages; 19 were ''upwelling'' Kelvin waves, generated by easterly wind events and linked to shoaling of the thermocline and cool temperature anomalies in the ITF. Both downwelling and upwelling Kelvin waves have similar vertical structures in the ITF outflow passages, with strong transport anomalies over all depths and a distinctive upward tilt to the phase that indicates downward energy propagation. A linear wind-forced model shows that the first two baroclinic modes account for most of the intraseasonal variance in the ITF outflow passages associated with Kelvin waves and highlights the importance of winds both in the eastern equatorial Indian Ocean and along the coast of Sumatra and Java for exciting Kelvin waves.

Using SLA as a proxy for Kelvin wave energy shows that 37% ± 9% of the incoming Kelvin wave energy from the Indian Ocean bypasses the gap in the coastal waveguide at Lombok Strait and continues eastward. Of the energy that continues eastward downstream of Lombok Strait, the Kelvin waves are split by Sumba Island, with roughly equal energy going north and south to enter the Savu Sea.

1. Introduction

The Indonesian Throughflow (ITF), the flow of water from the Pacific into the Indian Ocean through the narrow passages of the Indonesian archipelago, is an important conduit for mass, heat, and freshwater between the two ocean basins. The ITF is thought to impact global circulation of both the ocean (Song et al. 2004) and atmosphere (Schneider 1998). The ITF is highly variable across a broad range of frequencies, and there is a complicated interplay between locally and remotely forced energy (Wijffels and Meyers 2004). The variability in the intraseasonal band (30–90 days) is particularly striking. Although some intraseasonal energy in the ITF exit passages originates from local and remote Pacific Ocean winds (Qiu et al. 1999; Schiller et al. 2010), the majority of the energy is forced remotely by wind anomalies over the Indian Ocean, which excite Kelvin waves that propagate eastward along the equator to the Indonesian coast and then on into the ITF region as coastally trapped Kelvin waves (Potemra et al. 2002; Wijffels and Meyers 2004).

Kelvin waves transmit energy downward from the sea surface, so quantifying their subsurface structure (e.g., baroclinic mode number, vertical energy propagation) is critical to understanding how remote Indian Ocean winds affect the ITF interior. The impact that Kelvin waves have on the ITF is largely unknown: the waves

Corresponding author address: Kyla Drushka, Scripps Institution of Oceanography, 9500 Gilman Dr., La Jolla, CA 92109-0230.
E-mail: kdrushka@ucsd.edu

DOI: 10.1175/2010JPO4380.1

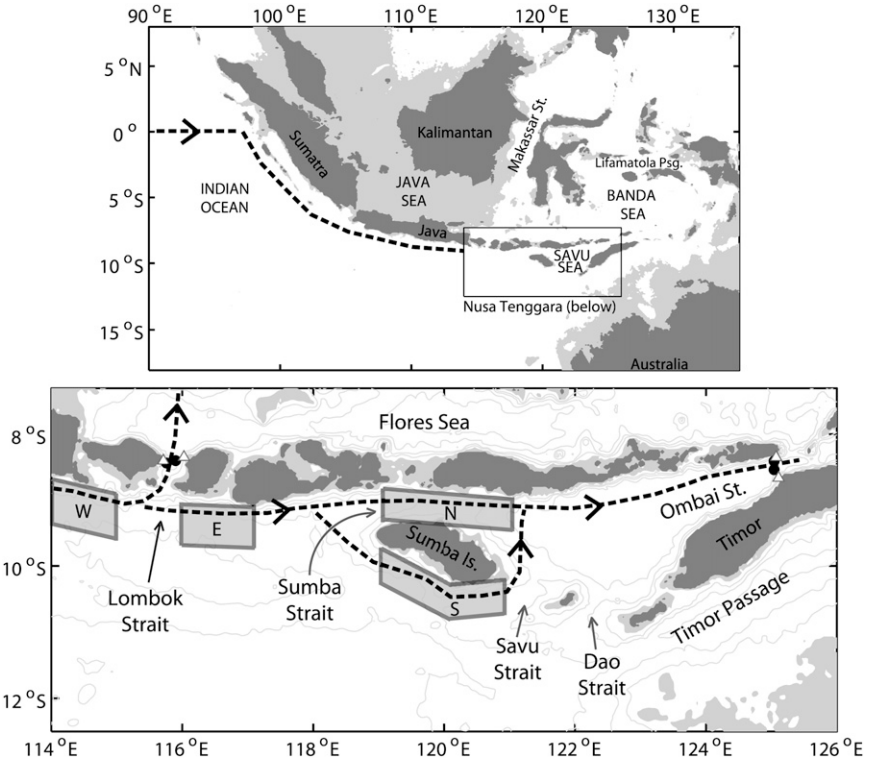

FIG. 1. (top) Indonesian archipelago. The 0–100-m depth is shaded in gray. (bottom) Nusa Tenggara region. Lombok and Ombai Strait moorings and pressure gauges with temperature sensors are indicated with circles and triangles, respectively. The 0–100-m depth is shaded in gray, and the 500-, 1000-, 2000-, and 4000-m contours are drawn in pale gray. The Kelvin wave path is shown as a dashed line. The *E* and *W* labels and shading refer to the regions east and west of Lombok Strait; *N* and *S* labels refer to the regions north and south of Sumba Island.

travel southeastward along Sumatra and Java, then reach the first significant gap in the coastal waveguide at Lombok Strait (Fig. 1). Theoretical (Durland and Qiu 2003; Johnson and Garrett 2006) and modeling (Qiu et al. 1999) studies have demonstrated that nearly all of the incoming intraseasonal Kelvin wave energy should enter Lombok Strait, but in situ observations have shown Kelvin wave energy in Ombai Strait (Molcard et al. 2001; Potemra et al. 2002; Sprintall et al. 2009, hereafter S09) and a recent modeling effort by Qu et al. (2008) demonstrated the same. Syamsudin et al. (2004) used altimetric data to estimate that 56% of incoming semiannual Kelvin wave energy enters Lombok Strait, but the amount of intraseasonal Kelvin wave energy entering Lombok Strait has not been well quantified with observations. Few in situ measurements have captured Kelvin waves in the Indonesian archipelago, and most of these have focused on the semiannual Kelvin waves forced during the monsoon transition seasons in May and November (Arief and Murray 1996; Sprintall et al. 1999, 2000; Hautala et al. 2001; Potemra et al. 2002). Little is known about the vertical profile of velocity associated with Kelvin waves (Wijffels and Meyers 2004), particularly in the Indonesian archipelago, which has many sills, islands, and other topographic features that likely affect local Kelvin wave dynamics (S09). Sprintall et al. (2000) used data from a pressure gauge array within the ITF outflow straits to observe the passage of a semiannual Kelvin wave; however, this dataset provided no information on the vertical structure of the Kelvin waves. Horii et al. (2008) observed the vertical velocity and temperature structures of Kelvin waves in the open ocean at a mooring in the eastern equatorial Indian Ocean and found a clear pattern of positive and negative velocity and temperature anomalies associated with Kelvin waves forced by periodic Indian Ocean winds.

In this paper, we examine how Kelvin waves propagate through the Indonesian archipelago by using observations from the International Nusantara Stratification and Transport (INSTANT) project, a 3-yr deployment of moorings and pressure gauges in the straits of Indonesia designed to measure the ITF (Sprintall et al. 2004). This is a unique dataset for observing Kelvin waves in this region: INSTANT provides a long time series of full-depth

direct current measurements in the ITF outflow passages, allowing for the first time the subsurface structures of Kelvin waves to be observed and characterized in terms of their vertical energy propagation, baroclinic modes, and interaction with topography. Here, we use the INSTANT velocity and temperature measurements made during 2004–06 in two ITF outflow passages, the Lombok and Ombai Straits, to characterize the vertical structure of ITF Kelvin waves, their interaction with the regional topography, and their links to Indian Ocean wind forcing. A linear wind-forced model is used to evaluate the hypotheses motivated by the observations.

2. Datasets

a. INSTANT

The aim of the INSTANT project was to make direct full-depth measurements of the velocity and temperature structure of the ITF to quantify its mass and heat transports and to understand its variability on intraseasonal, seasonal, and annual time scales (Sprintall et al. 2004). The INSTANT array consisted of 11 deep moorings in the major inflow (Makassar and Lifamatola; see Fig. 1; Gordon et al. 2008; van Aken et al. 2009) and outflow (Lombok, Ombai, and Timor) passages of the ITF (S09), plus shallow coastal pressure gauges deployed on either side of each of the outflow passages (Drushka et al. 2008). In this study, we use mooring data from the Lombok and Ombai Straits. The moorings were deployed in December 2003–January 2004, recovered and redeployed in June–July 2005, and recovered in November–December 2006. Detailed descriptions of the mooring configuration, deployment, and data processing are given by S09.

The two Lombok Strait moorings were located on each side of the 35-km-wide, roughly north–south-oriented passage, in deeper water just north of the 300-m sill (Fig. 1). The two Ombai Strait moorings were located on either side of the 37-km-wide, east–west-oriented passage. In both passages, the subsurface mooring configurations were similar, with an upward-looking ADCP positioned to capture the surface flow above ~300 m and current meters positioned at discrete depths below. All measurements were objectively mapped onto hourly grids with 10-m depth spacing.

The Lombok West mooring was not recovered in December 2006, and data at this location are only available for the first 18 months of the INSTANT deployment period. However, the complete 3-yr time series at Lombok East is available. The first 18 months of data at Lombok East are well correlated with the measurements from the Lombok West mooring, allowing the second 18 months of data at Lombok West to be predicted from the Lombok East data (see S09 for details).

Transports Q were computed by interpolating the along-strait velocities at each time and depth to a cross-strait grid, assuming no-slip conditions at the bottom and sidewalls, and then summing over the width of the strait to obtain a value of along-strait transport at each time and depth. At each depth, the transport anomaly Q' was computed with respect to the mean at that depth over the entire time series. S09 used the range of values determined from several different interpolation schemes to provide uncertainties for the transport measurements. They estimated 25%–30% uncertainty on the total Lombok Strait transports and up to 45% on the Ombai Strait total transport. Here, we use the same interpolation schemes as S09 and calculate the variance of the intraseasonally bandpassed data for each scheme. Based on this range, we estimate similar uncertainties on the intraseasonal transports: around 25% on the Lombok Strait transports and 45% on the Ombai Strait transports.

It is difficult to maintain surface moorings in the Indonesian straits because of pressures from fishing and other maritime activities, so no sensors were deployed above 100–200 m. None of the salinity sensors returned viable data, so this analysis is restricted to velocity and temperature observations. The width of the straits is much smaller than the Rossby deformation radius in this region (~100 km), so Kelvin waves are expected to have a similar effect on both sides of the straits and it is reasonable to use a single instrument to quantify the Kelvin wave signal within each strait. This was confirmed: the temperature trends associated with Kelvin waves were the same at both moorings in each strait, and our findings were not sensitive to the choice of mooring that was used to represent the temperature of each strait. We thus used temperatures from the mooring in each strait with the most complete record: 100 m and deeper at Lombok East and 200–1050 m at Ombai North. Coastal temperature sensors deployed in each strait at around 10-m water depth as part of a shallow pressure gauge array (Drushka et al. 2008) were also examined. However, the signals in these data associated with the Kelvin waves were less clear, likely because the measurements were influenced by coastal and tidal processes, and they are not used in this analysis.

b. Other data

Kelvin waves have a sea level anomaly (SLA) signature in the equatorial Indian Ocean on the order of 20 cm (Syamsudin et al. 2004). With phase speeds of 1–3 m s^{-1}, they take around 20 days to propagate across the Indian Ocean and around 10 days to travel along the Indonesian coast. Tracking the Kelvin waves eastward

along the equator from their generation region and then along coastal Sumatra and Java (Fig. 1) can be accomplished effectively using satellite altimetry. However, using altimetry to track Kelvin waves east of Lombok Strait, either into the internal Indonesian seas or along Nusa Tenggara, is complicated. The altimetric data are contaminated by land, so it is difficult to observe the Kelvin waves once they reach the many islands and narrow straits that make up the archipelago. There is also significant tidal aliasing of altimeter data at time periods of ~60 days (Stammer and Wunsch 1999), which further complicates quantifying intraseasonal signals in regions where the tide models may be imperfect. We explored the possibility that the raw, along-track altimetric sea surface height anomaly data [reference SLA, available from Archiving, Validation, and Interpretation of Satellite Oceanographic data (AVISO); Ducet et al. 2000] could offer additional insights compared to the gridded data (AVISO merged, updated SLA). In all of the analyses, there were no significant differences between the two altimetric products. The smoother gridded data are easier to visualize and so those results are presented here. These data are weekly, 0.25° × 0.25° gridded SLA, available for the period from October 1992 to the present.

Scatterometer winds were used to observe the forcing of Kelvin waves over the Indian Ocean. We used the level 3.0 six-hourly gridded dataset produced by the Global Modeling and Assimilation Office at the National Aeronautics and Space Administration (NASA) Goddard Space Flight Center. The product uses a variational analysis method to combine data from several satellite missions, and it is available globally on a 25 km × 25 km grid (Ardizzone et al. 2009).

Indian Ocean temperature and salinity measurements from Argo, available as a gridded product with 30 day × 1° horizontal resolution × 10–100 m vertical resolution, were also used (Roemmich and Gilson 2009). These data are too coarse to resolve the propagation of Kelvin waves along their path, but they provide a measure of both the background stratification as well as its seasonal and spatial variations.

3. Background

a. Wind forcing

Kelvin waves are forced by wind anomalies over the ocean. Westerly wind anomalies produce disturbances that depress the thermocline and thus are commonly referred to as downwelling Kelvin waves. These increase the upper-ocean temperature in the eastern part of the basin both by advecting warm water east and by reducing the upwelling of colder water (Giese and Harrison 1990). In the Indian Ocean, anomalous westerly winds occur at both semiannual and intraseasonal frequencies (Potemra et al. 2002). The mechanisms underlying the forcing at these frequencies are fundamentally different: during the monsoon transition seasons, roughly in May and November, westerly wind anomalies over the central part of the Indian Ocean force a semiannual Kelvin wave, commonly referred to as the Wyrtki jet (Wyrtki 1973). Independently, intraseasonal westerly wind anomalies arise from the Madden–Julian oscillation (MJO), a coupled ocean–atmosphere phenomenon consisting of large-scale patterns of convection that propagate eastward across the Indian and Pacific Oceans (Madden and Julian 1971; Zhang 2005). In this study, the semiannual harmonics have been removed from all data to restrict the analysis to the intraseasonal Kelvin waves.

Intraseasonal easterly wind anomalies force upwelling Kelvin waves that are manifested as eastward-propagating anomalies that shoal the thermocline depth. The result is a shallow thermocline off the coast of Sumatra, which enhances the upwelling of cool deep water and directly lowers the temperature in the upper layer (Yu and Rienecker 1999). Thus, oscillating intraseasonal winds over the Indian Ocean are expected to produce alternating warm, downwelling and cold, upwelling Kelvin waves (Masumoto et al. 2005). Cool sea surface temperature (SST) anomalies in the eastern Indian Ocean have been linked to the development of Indian Ocean dipole (IOD) events (e.g., Yu and Rienecker 2000; Han et al. 2006; Vinayachandran et al. 2007; Horii et al. 2008). The IOD is characterized by a strong SST gradient across the Indian Ocean, with anomalously cool SSTs seen in the eastern Indian Ocean off Sumatra during its positive phase (Saji et al. 1999). Interannual variations such as the IOD may also affect intraseasonal dynamics of the Indian Ocean (Rao et al. 2007). Although a strong IOD occurred in 2006 during the INSTANT period, the present study is restricted to intraseasonal variability in the ITF; interannual variations and their relationship to intraseasonal Kelvin waves will be the subject of a future study.

b. Kelvin wave vertical structures

Both downwelling and upwelling wind-forced Kelvin waves can be thought of as a superposition of vertical modes that combine in such a way that energy and phase propagate both horizontally and vertically, carrying energy into the ocean interior with a slope that can be predicted by linear inviscid ray theory (McCreary 1984). We consider our observations in this context to 1) assess how well they are described by linear theory, 2) estimate the dominant modal structures of the Kelvin waves, and 3) evaluate the interaction between vertical energy

TABLE 1. The mean theoretical Kelvin wave phase speeds $\bar{c}$ and standard deviation σ_c, averaged across the equatorial Indian Ocean and the INSTANT deployment period, for the first three modes. Also given is the approximate time for each Kelvin wave mode to travel from Lombok to Ombai Strait.

n	$\bar{c}$ (m s^{-1})	σ_c (m s^{-1})	Lombok–Ombai time (days)
1	2.83	0.20	4.7
2	1.80	0.14	7.7
3	1.26	0.15	11.8

propagation and the topography of the Indonesian archipelago.

From the linearized shallow water equations, each baroclinic mode-n Kelvin wave can be described by

$$\frac{\partial}{\partial z}\left[\frac{1}{N(z)^2}\frac{\partial \psi_n(z)}{\partial z}\right] = -\frac{1}{c_n^2}\psi_n(z), \qquad (1)$$

subject to the boundary conditions

$$\frac{\partial \psi_n(0)}{\partial z} = \frac{\partial \psi_n(H)}{\partial z} = 0,$$

and normalized such that

$$\int_{-H}^{0} \psi_n^2(z)\, dz = H,$$

where ψ_n is the mode-n vertical structure function; c_n is the phase speed of that mode; $N(z)$ is the Brunt–Väisälä frequency, assumed to vary only with depth; and H is the bottom depth (McCreary 1984; Cane 1984). Note that ψ represents the horizontal velocity. By solving Eq. (1) as an eigenvalue problem for a given stratification $N(z)$, the expected vertical structure and phase speed for each mode can be computed. Here, we use the stratification from the gridded Argo temperature and salinity fields: the expected phase speeds for the first three modes are presented in Table 1, with the mean and standard deviation values based on the range of stratifications observed across the equatorial Indian Ocean (2°S–2°N, 45°–99°E) during the 2004–06 INSTANT deployment period. Table 1 also contains the approximate travel time for each mode to propagate along the coastal waveguide from Lombok to Ombai Strait, based on the phase speed calculated from the stratification in the Nusa Tenggara region (9°S, 115°–125°E) and assuming a distance of ~1050 km between the Lombok and Ombai Straits (Fig. 1). The first three vertical structure functions, based on average Indian Ocean stratification, are plotted in Fig. 2: the first baroclinic mode is positive down to 1500-m depth, whereas the second baroclinic mode has a zero crossing at around 200 m. The third mode has zero crossings at around 100 and 900 m. Although McCreary (1984) suggests that the superposition of many higher-order modes is required for Kelvin wave energy to propagate as a beam of energy into the ocean interior, observations of Pacific and Indian Ocean Kelvin waves have shown that, in practice, only the lowest two or three modes are distinguishable and significant in large-scale Kelvin wave dynamics (e.g., Eriksen et al. 1983; Giese and Harrison 1990; Cravatte et al. 2003).

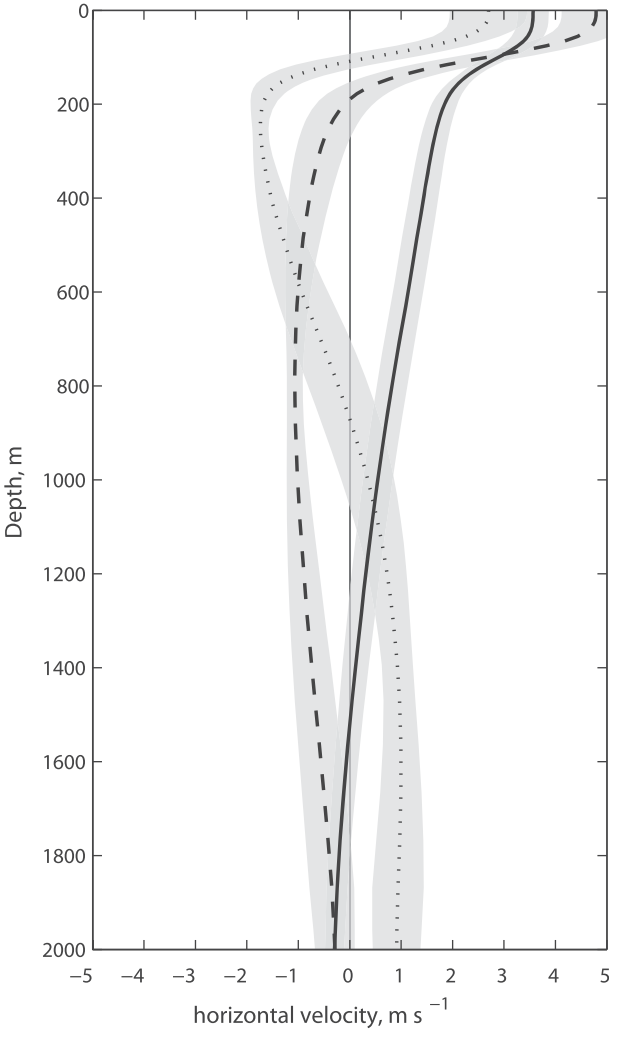

FIG. 2. Theoretical vertical structure functions $\psi(z)$ of Indian Ocean Kelvin waves. The first, second, and third modes are plotted as solid, dashed, and dotted lines, respectively, and 1σ error bars are shaded. The functions represent horizontal velocity and are normalized according to Eq. (1).

Linear ray theory, which arises from the Wentzel–Kramers–Brillouin (WKB) approximation that stratification $N(z)$ varies slowly with respect to the vertical wavelength of the wave, states that Kelvin wave energy propagates in the vertical at an angle θ,

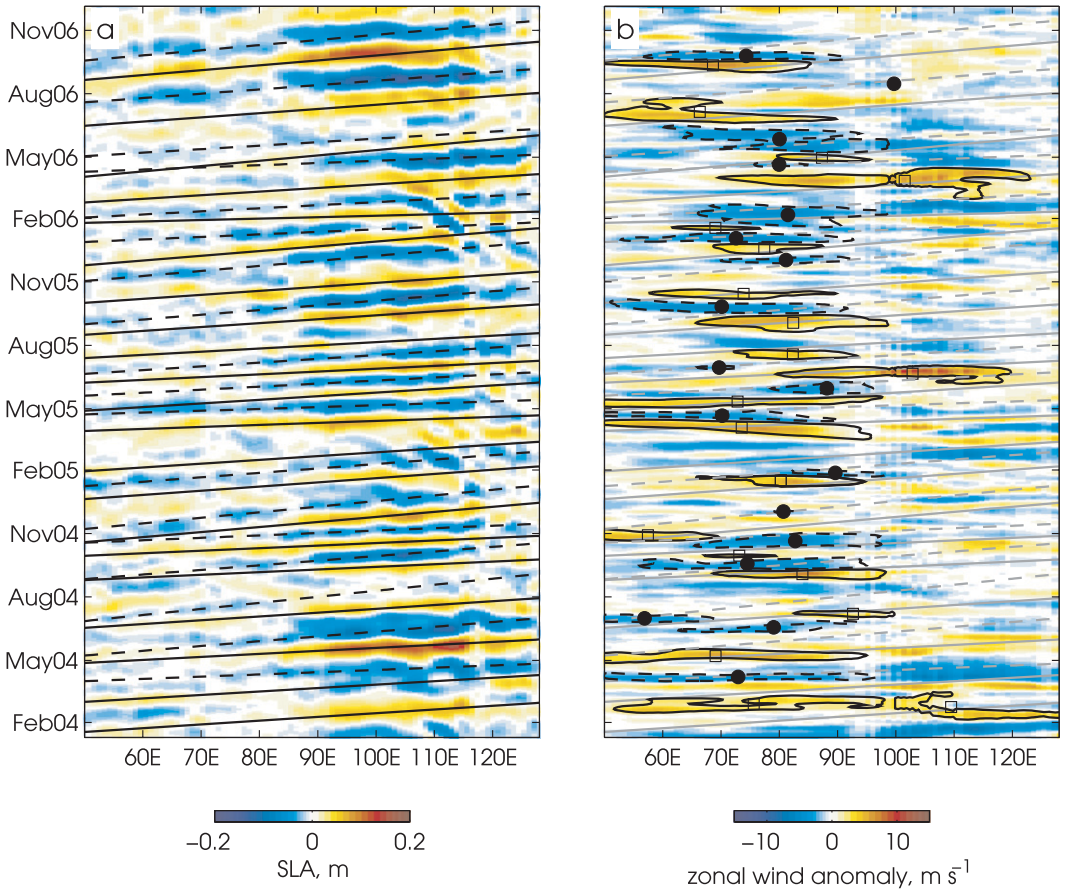

FIG. 3. Time–longitude plots of (a) SLA and (b) anomalous alongshore winds. The x axis corresponds to longitudes along the path assumed to have been taken by the Kelvin waves (dashed line in Fig. 1). The straight lines show the fits to the Kelvin wave SLA signals, with solid lines indicating downwelling events and dashed lines indicating upwelling events. The contours in (b) indicate the wind signals associated with the Kelvin waves, with westerly wind anomalies (>2 m s^{-1}) contoured with solid lines and easterly wind anomalies (<-2 m s^{-1}) contoured in dashed lines. The centers of the westerly and easterly wind bursts are plotted as squares and circles, respectively.

$$\theta(z) = \frac{dz}{dx} = \frac{-\omega}{N(z)}, \tag{2}$$

where ω is the frequency of the wind forcing. This was first applied to the case of Indian Ocean Kelvin waves by Luyten and Roemmich (1982), who showed that semiannual Kelvin waves forced by winds anywhere in the equatorial Indian Ocean will reach Sumatra in the top 200 m of the water column. Generally, Eq. (2) suggests that higher-frequency energy can ''dive'' deeper than lower-frequency energy and that, the farther west a Kelvin wave is generated in the equatorial Indian Ocean, the deeper it will have penetrated before reaching a given longitude to the east. This becomes particularly important when considering Kelvin wave propagation through the ITF region, where there are many shallow sills, islands, and bathymetric features that could affect wave dynamics at depth. On the basis of the Argo stratification, Eq. (2) predicts that a Kelvin wave at a 45-day period generated at 60°E on the equator in the Indian Ocean will have dived to around 2500 m by the time it reaches Lombok Strait, whereas a wave originating at 85°E will only have reached 1000 m. Kelvin waves generated at 80°E must be forced at periods longer than around 90 days to penetrate no deeper than the 300-m sill depth at Lombok Strait and at periods longer than around 65 days to penetrate shallower than the ~900-m sill north of Sumba Island to reach Ombai Strait (Fig. 1).

4. Observations of Kelvin waves

a. Sea level anomalies

Figure 3a shows a Hovmöller diagram of altimetric SLA over the Indian Ocean and following the Kelvin wave path along the Sumatra and Java coasts (Fig. 1).

The annual and semiannual harmonics were removed and the data were bandpassed with a 30–90-day filter, revealing a series of coherent eastward-propagating positive and negative SLA signals corresponding to downwelling and upwelling Kelvin waves, respectively. Generally, positive and negative SLA events alternate, consistent with them being forced by periodic winds. Except for their sign, downwelling and upwelling Kelvin waves share similar characteristics in their SLA signals: the magnitude of the SLA signals increases toward the east, consistent with them being forced by a patch of wind with a large fetch, and the largest SLA values are seen along the coast of Sumatra. Farther east along the Kelvin wave path in the Nusa Tenggara region (Fig. 1), the SLA signal appears to decrease. This may partly be an artifact of the sparser altimeter data within the Indonesian islands. It may also indicate that the Kelvin wave energy is being dissipated on the topography, reflected, or routed along a different pathway (e.g., northward along the western coast of Sumatra). There are a number of instances of westward-propagating SLA signals east of ~105°E: for example, around February 2006 (Fig. 3a), which are likely Rossby waves that originate as reflected Kelvin waves. These signals propagate at around 0.3 m s^{-1}, consistent with previous observations of Rossby waves in this region (Peter and Mizuno 2000). The trace of the signals is not seen west of the bend in the coastal waveguide where Sumatra and Java meet. This suggests that the reflected Rossby waves travel along the coast of Java and then continue propagating westward into the Indian Ocean at this latitude.

To quantify the properties of the individual Kelvin waves, we used an objective procedure to pick each event out of the SLA data based on Fig. 3a. Note that, for all of the steps in the extraction of the Kelvin wave signals, the same procedure was used to isolate the downwelling (positive SLA) and upwelling (negative SLA) Kelvin waves. First, the positive and negative SLA peaks at longitude 95°E having an amplitude of at least 1 cm were identified as ''events.'' This longitude was used to define the Kelvin wave events because the intraseasonal SLA variability there is high and is well correlated with signals to the east and west of it, suggesting that SLA at this longitude captures the intraseasonal Kelvin wave effectively. From the SLA peaks at 95°E, we identified 22 downwelling and 21 upwelling Kelvin waves during the 2004–06 INSTANT time period. For each of these events, a series of coherent, eastward-propagating SLA peaks with an amplitude of at least 1 cm were identified along the Kelvin wave path, and a line was fit to the SLA peaks to estimate the propagation speed and its uncertainty (lines in Fig. 3). The phase speeds estimated from the SLA range from 1.6 to 6.1 m s^{-1}, with an average value of 2.6 ± 1.0 m s^{-1} (Fig. 4). The phase speeds for downwelling and upwelling events are in agreement. The phase speeds for all events are in a range consistent with Kelvin waves of the first three modes (Table 1). However, there is not a distinctive separation between the modes, likely because the observed waves are a superposition of two or more modes. In addition, there are limitations on the precision of estimating phase speed from SLA: bandpass filtering the data, which is necessary to isolate coherent SLA events, erodes the precision of the phase speed estimate. However, the robustness of the phase speed estimates across the set of events, as well as their agreement with theory, indicates that the range of values is reasonable.

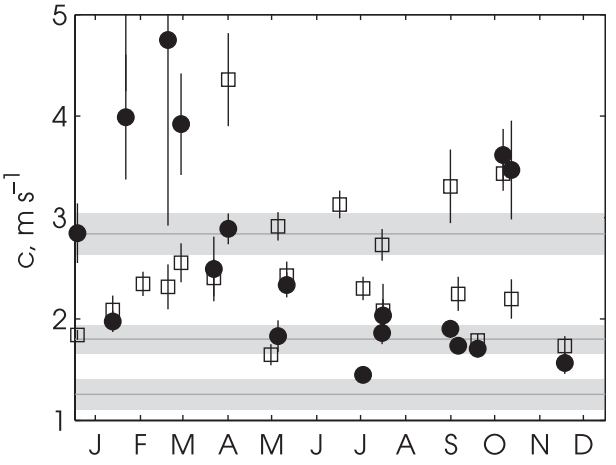

FIG. 4. Kelvin wave phase speeds and uncertainties estimated from SLA for downwelling (squares) and upwelling (circles) events, plotted against month. Error bars are from the linear fit to the SLA data. Horizontal gray areas indicate the theoretical phase speeds for the first three modes of Indian Ocean Kelvin waves, with uncertainties, during the INSTANT time period (Table 1).

b. *Transport observations in the ITF outflow passages*

Figure 5 shows the mean and anomalous transports through the Lombok and Ombai Straits. The mean flow through both straits was toward the Indian Ocean, roughly southward in Lombok Strait and westward in Ombai Strait (Figs. 5a,b). Averaged over the INSTANT deployment, the total transports were −2.3 Sv (1 Sv ≡ 10^6 m^3 s^{-1}) through Lombok Strait (0–300 m) and −4.6 Sv through Ombai Strait (0–1600 m). Timor Passage (Fig. 1) carried an additional −7.5 Sv (S09) for a total ITF transport of −14.4 Sv toward the Indian Ocean. The anomalous transports were bandpassed with a 20–365-day Butterworth filter to remove the high-frequency (primarily diurnal) and interannual signals, and the annual and semiannual harmonic at each depth

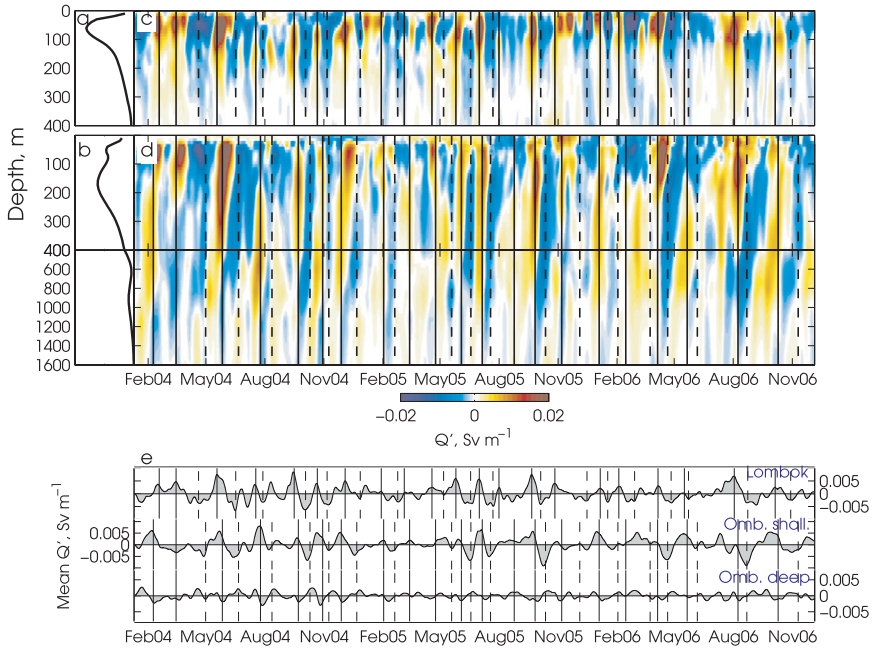

FIG. 5. Mean transports (Sv per unit depth) through the (a) Lombok and (b) Ombai Straits; transport anomalies (Sv per unit depth) in the (c) Lombok and (d) Ombai Straits; and (e) depth-averaged transports in Lombok (averaged over depths 120–250 m) and Ombai shallow (250–800 m) and deep (1200–1900 m). Negative values indicate ITF outflow. Vertical lines indicate the times the Kelvin waves observed in this study passed through each strait: solid lines denote downwelling waves and dotted lines denote upwelling waves. In Lombok Strait, these lines correspond to the peak transport anomaly at 130 m; at Ombai Strait, the lines correspond to the peak at 230 m. Note the two depth scales in (b) and (d).

was removed to concentrate on intraseasonal rather than semiannual Kelvin waves.

The transport anomalies (Figs. 5c,d) are highly energetic throughout the water column. In both passages, there is strong variability in the mixed layer to ~100-m depth, likely because of local fluctuations in wind (Schiller et al. 2010). Deeper, there are episodic positive and negative anomalies in the flow through both straits, distinctive events that persist for a few days or longer. Many of the reversals observed in Ombai Strait occur several days after a reversal is observed in Lombok Strait, suggesting features propagating eastward at phase speeds on the order of 1–4 m s^{-1}, consistent with low-mode baroclinic Kelvin waves (Table 1).

A lag-correlation analysis confirms that intraseasonal transport anomalies propagate eastward from Lombok to Ombai. Because energy is traveling in the vertical [Eq. (2)] as well as the horizontal, a Kelvin wave transport anomaly that is seen at a certain depth in Lombok Strait may be seen at a different depth in Ombai Strait. Thus, although the signals are propagating eastward, a Kelvin wave can be observed earlier at depth in Ombai Strait than nearer the surface in Lombok Strait. The lag-correlation analysis shows that Lombok Strait transport anomalies at 200-m depth lead Ombai Strait transport anomalies at 200-m depth by 7 days, comparable to the travel times expected for low-mode Kelvin waves to travel from Lombok to Ombai Strait (Table 1). However, 200-m depth Lombok Strait transport anomalies lead 500-m Ombai Strait transport anomalies by just 1 day; that is, as the Kelvin waves dive, the deep lag-correlated signal reaches Ombai earlier than the shallow signal. This confirms the expectation that energy is propagating vertically but makes it complicated to use the lags to precisely estimate the phase speed of the Kelvin waves.

To observe subsurface Kelvin wave signatures in the ITF outflow passages, we linked each of the SLA events identified above to a signal in Lombok and Ombai Strait transport anomalies. For each SLA event, the associated transport anomaly peak in each strait was selected with an objective two-step procedure, with positive SLA peaks matched to positive transport anomalies (downwelling Kelvin waves) and negative SLA peaks matched to negative transport anomalies (upwelling Kelvin waves). First, the line fit to the SLA data was used to predict when each Kelvin wave was expected to arrive at each strait. As discussed above, the subsurface Kelvin wave structure is sloped, so there is a time lag between the arrival of the

surface and subsurface Kelvin wave signals: for first-mode and second-mode intraseasonal waves, the arrival at 200–1000-m depth in the outflow passages should lead the surface arrival by around 2–20 days [Eq. (2)]. Thus, to match the signals in transport and SLA, we looked for subsurface transport anomaly signals arriving at the Lombok and Ombai Straits within the 20-day period preceding the surface SLA signals.

In Lombok Strait, the timing of the events that were defined as Kelvin waves corresponds to the peaks in transport anomalies averaged over depths 120–250 m (Fig. 5e). In Ombai Strait, some events only appear in shallower water and some only appear at depth. Most events are seen throughout the water column, although there is often a discontinuity between the shallow and deep signals (Fig. 5d). As noted by S09, the distinction between the shallow (down to ~900 m) and deeper (below ~1200 m) transport anomaly signals in Ombai Strait may be due to the sills north (900 m) and south (1150 m) of Sumba Island, which control the deep flow between the Lombok and Ombai Straits (Fig. 1). The deep Kelvin wave energy may be trapped below the 900-m Sumba sill and propagate south rather than north of Sumba Island before reaching Ombai Strait. For this reason, we used two separate depth ranges to identify Kelvin wave reversals in Ombai Strait: 250–800 m ("shallow") and 1200–1800 m ("deep"). The depth-averaged transport anomalies are shown in Fig. 5e. Of the 43 Kelvin wave events observed in SLA, there were 2 strictly deep events, 17 strictly shallow events, and 21 events with both shallow and deep signals (vertical lines in Figs. 5d,e). Three Indian Ocean SLA events (Fig. 3a) could not be definitively linked to transport events in the Lombok and/or Ombai Straits, and they have been excluded from the analysis. We considered a total of 40 events, 21 downwelling and 19 upwelling, for the remainder of the study. There are around five transport anomalies in Figs. 5b,d that appear Kelvin wave–like but have not been linked to Indian Ocean SLA events and are not included in this analysis (e.g., positive transport anomaly in August 2004). These signals may be due to energy from local winds or remote Pacific Ocean winds, or they may be Kelvin waves with weak or convoluted SLA signals in the Indian Ocean that were not captured by the scheme we used to identify events.

For both downwelling (positive transport anomaly) and upwelling (negative transport anomaly) events, the upward phase propagation can be seen as a shoaling of the Kelvin wave signal with time in the anomalous transport time series (Figs. 5c,d), particularly at Ombai Strait. This is consistent with the expectation of Kelvin waves forced at the surface to have downward-propagating energy and upward-propagating phase. From Eq. (2), the forcing frequency ω can be estimated if the stratification $N(z)$ and the angle of propagation θ are known, based on the relationship

$$\omega(z) = -N(z)\theta = -N(z)\frac{dz}{dx} = -N(z)\frac{\dfrac{dz}{dt}}{\dfrac{dx}{dt}} = -N(z)\frac{\dfrac{dz}{dt}}{c}. \tag{3}$$

The stratification $N(z)$ obtained from the Argo data was used with Eq. (1) to estimate the phase speed c_n in the Nusa Tenggara region (Fig. 1), and the peak Q' from the transport anomalies for each event (Figs. 5c,d) were used to estimate dz/dt at each depth. From Eq. (3) we then estimated the average frequency of the wind forcing $\omega(z)$ for the Kelvin waves at each depth based on the local phase slope and the local stratification, and the mean ω was estimated by averaging over depths 100–300 m in Lombok Strait and 200–1200 m in Ombai Strait. From the 40 observed downwelling and upwelling events, we estimate from the Lombok Strait transports that the Kelvin waves are forced by winds with a period of 28 ± 15 days, with the uncertainty representing one standard deviation. The Ombai Strait transport anomalies give an estimate that the Kelvin waves are forced by winds with a period of 46 ± 18 days. These estimates are consistent with intraseasonal wind forcing, albeit with a large uncertainty, suggesting that it is reasonable to use linear theory to describe the upward phase propagation of Kelvin waves observed in the ITF. The discrepancy in the Lombok and Ombai estimates likely results from the difficulty in estimating dz/dt in the Lombok Strait signals, which have probably had their structures modified as a result of the topography of Lombok Strait. Note that the estimates are based on the mode-1 phase speed. From Eq. (3), it can be seen that forcing frequency is inversely proportional to phase speed; so, because $c_2/c_1 \sim 0.6$ (Table 1), the wind forcing period could conceivably be around 60% of these values, which is in the lower range of the intraseasonal band. This method is based solely on the local observations in the ITF passages, and thus represents an independent estimate of the prevailing frequency of Indian Ocean winds that force Kelvin waves.

Composites of the Kelvin wave transport anomalies were constructed by isolating each Kelvin wave in the transport anomaly time series (Figs. 5c,d) and then averaging over the set of events. For each event, $t = 0$ was defined as the time of the peak transport anomaly associated with that event, at 130 m in Lombok Strait and at 230 m in Ombai Strait. Then, the full-depth anomaly for the $t = \pm 15$ days was extracted to give a picture of the depth–time structure. Separate composites were formed for the set of downwelling events and the set of upwelling

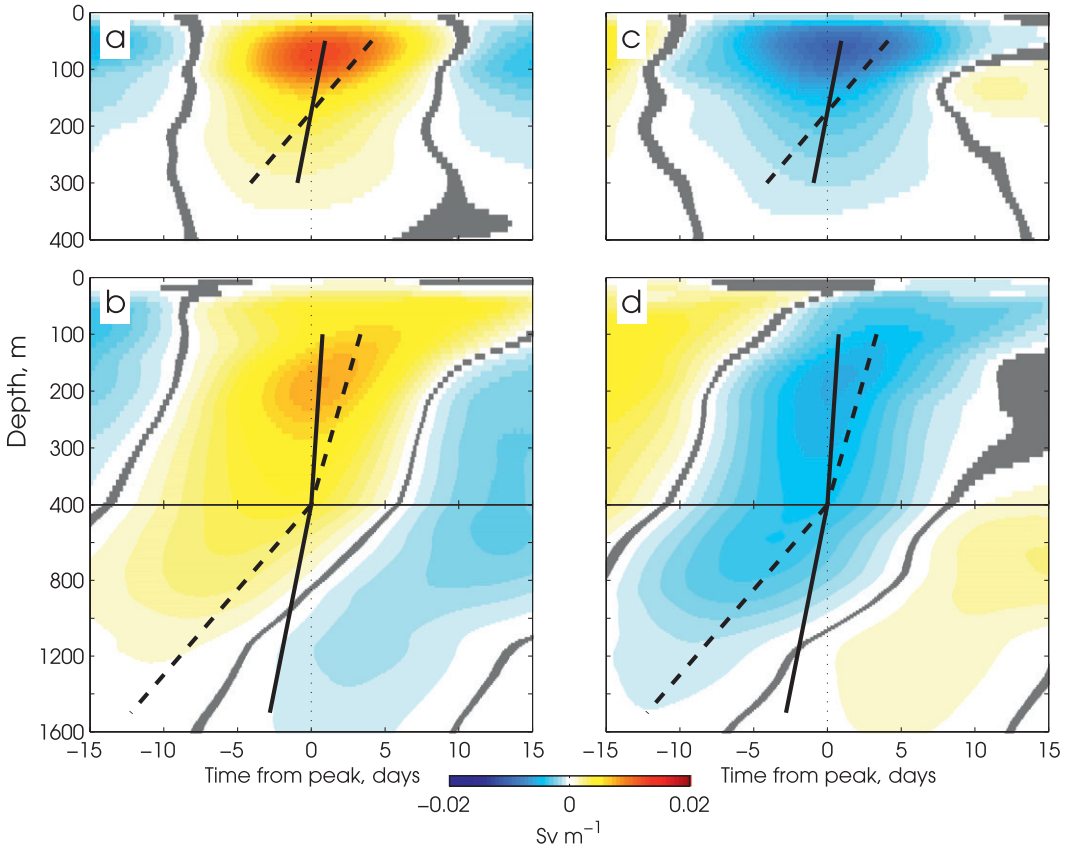

FIG. 6. Composites of transport anomalies (Sv m^{-1}) for (a),(b) downwelling and (c),(d) upwelling Kelvin waves in the (a),(c) Lombok and (b),(d) Ombai Straits. Areas where the mean is less than the standard error have been masked out. The solid and dashed lines represent the approximate phase slope for Kelvin waves forced by winds with periods of 12 and 54 days, respectively. These value are the minimum and maximum values of the forcing period (mean ± standard deviation) estimated from the transports. Note the two vertical scales in (b) and (d).

events, for both the Lombok and Ombai Strait data (Fig. 6). To evaluate whether the transport anomaly composites for the downwelling and upwelling events were statistically distinct from each other, a Monte Carlo simulation was performed. Drawing from the 40 available Kelvin wave events, two transport composites were formed for both Lombok and Ombai Strait data, one from a random selection of 21 events and the other from the remaining 19 events. Then the root-mean-square difference (RMSD) between the pair of composites was used as a metric for "distinctiveness." The test was performed for 1000 random composite pairs and the RMSD values compared to the RMSD of the actual composites for both locations. The RMSD of the downwelling and upwelling transport anomaly composites was found to be greater than the RMSD of the random pair more than 95% of the time, indicating that the differences observed between the downwelling and upwelling waves are significant.

Apart from their signs, the structures of the transport composites of the downwelling and the upwelling events are similar (Fig. 6). The transport anomalies are strongest at depths above the controlling sills in each strait, 300 m in Lombok and 900–1150 m in Ombai, as expected for signals arriving from the Indian Ocean (Fig. 1). For both the downwelling and upwelling events, the strongest transport anomalies are seen at around 70 m in Lombok Strait; at this depth, the Kelvin wave transport reversals persist for around 14 days in Lombok Strait and around 20 days in Ombai Strait. The positive transport anomaly of the downwelling events is preceded and followed by negative transport anomalies; similarly, the negative transport signal of the upwelling events is flanked by positive transport anomalies. This is a result of the periodic nature of intraseasonal Kelvin waves; based on each composite representing half a cycle, this points to a forcing period of 28–40 days, consistent with the values estimated completely independently from the vertical phase slopes. At Ombai Strait, the distinctive upward Kelvin wave phase propagation seen in the time series is captured in the composites. However, using the phase

slope of the composite transport anomalies to estimate the forcing frequency ω yielded values of 15 (Lombok) to 28 days (Ombai), around half of what was computed from the individual events above. This suggests that the averaging procedure used to form the composites smoothes over some of the detail in the vertical structures and that the Kelvin waves vary substantially from one event to the next. Thus, although composites are useful for observing the general subsurface properties of Kelvin waves, the events must be considered individually to understand their dynamics.

The composites presented in Fig. 6 provide a crude estimate of the magnitude of the Kelvin wave transports. We considered each event to be defined by the significant (with respect to the standard error) positive or negative (for downwelling or upwelling events, respectively) portion of its transport anomaly. We then summed over all depths and averaged over the duration of the event to get an estimate of the transport anomaly associated with each Kelvin wave. The mean and standard deviation of the total Kelvin wave transport anomaly was then computed by averaging over all events. The downwelling events have a transport anomaly of 0.8 ± 0.2 Sv in the top 300 m of Lombok Strait and 2.2 ± 0.2 Sv in the top 1600 m of Ombai Strait. For the upwelling events, the magnitudes of the significant Kelvin wave transports are in agreement, with -0.8 ± 0.2 Sv through Lombok Strait and -2.1 ± 0.2 Sv through Ombai Strait. The errors reported for these estimates only reflect variability over the set of events and not the uncertainty inherent in the method used to compute the transport anomalies.

To diagnose the relative contributions of the baroclinic modes to each wave, we compared the observed Lombok Strait profile of each Kelvin wave transport anomaly to the vertical structure functions [Fig. 2; Eq. (1)]. We used two methods to do this: first, fitting the observed transport profiles to the theoretical profiles using a least squares fit; second, computing which of the theoretical vertical structure functions accounted for more of the variance of the observations based on their correlation coefficients. These two methods gave consistent results. Of the 21 downwelling and 19 upwelling Kelvin waves, 7 of each type of event were dominated by the second baroclinic mode and the rest were dominated by the first baroclinic mode. As expected, the phase speeds of the mode-2 dominated events, as derived from fits to the SLA, are generally lower than those associated with the mode-1 dominated events. Interestingly, all of the mode-2 dominated events occurred during boreal summer (May–October). The reasons for this are unclear, although many studies of equatorial Indian Ocean Kelvin wave dynamics have noted seasonal asymmetries (e.g., Waliser et al. 2003; Iskandar et al. 2005, 2009). Iskandar et al. (2005) suggested that mode-1 Kelvin waves are more efficiently excited in regions where the thermocline is thick, whereas mode-2 waves are more efficiently excited when the thermocline is thin and sharp. However, we see the opposite pattern, with the mode-2 events preferentially forced when the thermocline is deep. Mode 2 is a resonant mode in the Indian Ocean because of the basin geometry (Han 2005; Fu 2007); however, the resonance seems to dominate at the 90-day period, substantially longer than we have observed here, so we cannot explain our observations using resonance.

c. *Temperature observations in the ITF outflow passages*

Figure 7 shows the anomalous temperature time series at the Lombok East and Ombai North moorings, with the missing surface and deep levels masked out. The data were bandpassed to 20–365 days and the annual and semiannual harmonics removed, as for the transport data. Interestingly, the annual temperature signal was about twice as large as the semiannual signal in Lombok Strait, whereas in Ombai Strait the semiannual signal was larger. Intraseasonal temperature variability is strong, with peaks ranging from $-2°$ to $+2°$C in Lombok Strait (Fig. 7a) and $-1°$ to $+2°$C in Ombai Strait (Fig. 7b). From Fig. 7, it can be seen that patterns in the temperature time series are similar to the patterns in the transport time series, with alternating warm and cold events. Thermocline deepening resulting from downwelling Kelvin waves is expected to cause warm temperature anomalies; similarly, upwelling Kelvin waves are expected to be linked to cool temperature anomalies (McCreary 1983; Yu and Rienecker 1999; Masumoto et al. 2005). Observational studies have shown that Kelvin wave temperature anomalies generally lag the transport anomalies (e.g., Romea and Allen 1983; Johnson and McPhaden 1993).

To explore the relationship between Kelvin wave transport and temperature anomalies, we formed composites of the temperature anomalies associated with the downwelling and upwelling Kelvin waves. For each event, we used the same $t = 0$ that was used for the transport composites: that is, the times of the peak transport anomaly at 130 m in Lombok Strait and at 230 m in Ombai Strait. The composited temperatures at the Lombok and Ombai Straits are shown in Fig. 8. If the assumption that Kelvin wave temperature anomalies lag the transport signals holds true, the downwelling and upwelling events are clearly linked to warm and cold temperature anomalies, respectively, consistent with expectations. The downwelling events have an average peak temperature anomaly of $+0.3°$C at around 150-m depth in Lombok Strait, and the upwelling events have

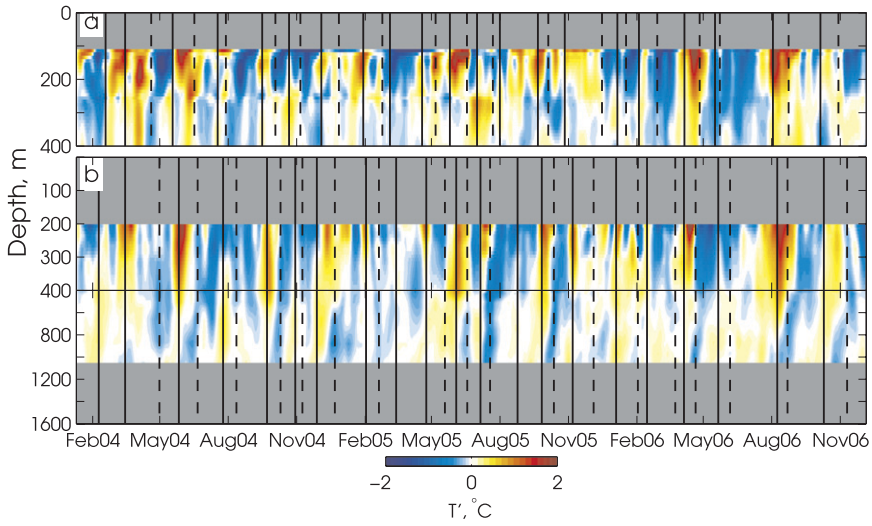

FIG. 7. Anomalous intraseasonal temperatures (°C) in the (a) Lombok and (b) Ombai Straits. Depths above the shallowest instrument and below the deepest instrument have been masked out. Vertical lines indicate the Kelvin wave arrivals inferred from the transport observations (Fig. 5): solid (dashed) lines denote downwelling (upwelling) waves. Note the two depth scales in (b).

an average temperature anomaly of −0.5°C at the same depth. The peak temperature anomalies probably lie above the shallowest level at which there are Ombai Strait data (Figs. 7b,d); however, in spite of the missing surface data, the Kelvin wave temperature structures are clear. As seen in the transport anomaly composites, the Lombok Strait Kelvin wave temperature anomalies are preceded and followed by anomalies of the opposite sign. The upward phase propagation apparent in the transport data (Fig. 6) is also seen in the temperature composites, although the slope is somewhat ambiguous. The timing of the peak temperature signal in relation to the peak transport signal ($t = 0$) is also ambiguous, with strong composite temperature anomalies in both straits seen from around $t = 2$–15 days. This suggests that the Kelvin wave temperature signals vary from event to event and that the averaging used to form the composite smears out the details of each temperature event. Indeed, a close comparison between the temperature anomalies and the timing of the transport anomalies (shading and vertical lines in Fig. 7) indicates that the relationship between Kelvin wave transport and temperature anomalies is not always straightforward. In some cases (e.g., February 2006), a warm event follows a downwelling event after a few days, and in other cases (e.g., February 2004), the time lag is 2 weeks. For some events (e.g., June 2006), the temperature anomalies are extremely weak. In some cases, the patterns seen at Lombok and Ombai Strait are also different: for example, in the March 2004 downwelling event, the lag between the transport and the temperature signal is close to 2 weeks in Lombok Strait but near zero in Ombai Strait (Fig. 7).

McPhaden (2002) used a mixed layer heat budget analysis to diagnose the phase relationship between Kelvin wave transport and temperature anomalies and noted that the exact phasing depends on the relative importance of the terms in the heat budget. For example, if horizontal advection dominates the Kelvin wave mixed layer temperature signal, the transport anomaly should lead the temperature anomaly by around one-quarter of a cycle; if Kelvin wave–induced vertical velocity variations control the mixed layer temperature, Kelvin wave transport and temperature anomalies should be in phase (McPhaden 2002). Unraveling the transport–temperature phase relationship in these observations is beyond the scope of this paper; however, we show that intraseasonal transport and temperature anomalies are linked using a lagged correlation analysis between transport and temperature anomalies at 130 m in Lombok Strait and at 230 m in Ombai Strait. At zero lag, the correlations between transport and temperature are low, with R^2 values of less than 0.05 in both straits. In Lombok Strait, temperature and transport anomalies have a maximum correlation ($R^2 = 0.19$, significant at the 95% level) for transport at 130 m, leading temperature at 130 m by around 15 days. In Ombai Strait, the maximum correlation ($R^2 = 0.29$) is seen for transport at 230 m, leading temperature at 230 m by around 6 days. For Kelvin waves with periods of around 30 days, these time lags are equivalent to phase lags of around ~180° at Lombok Strait and ~70° at Ombai Strait, suggesting the

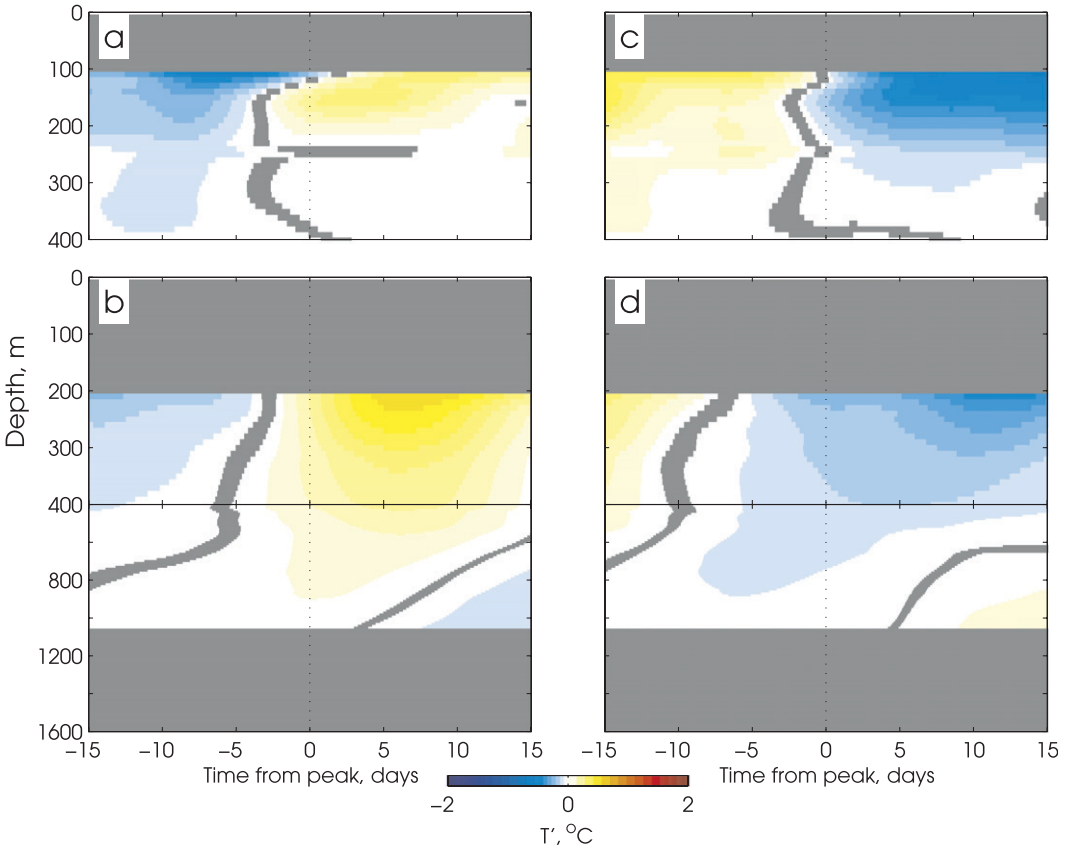

FIG. 8. As in Fig. 6, but for anomalous temperatures (°C). Depths above the shallowest instrument and below the deepest instrument have been masked out.

importance of horizontal advection in controlling the Kelvin wave temperature signal (McPhaden 2002). The significant lagged correlation between the time series of temperature and transport anomalies motivates us to look for relationships between the anomalies for the individual Kelvin wave events. For each Kelvin wave event, we found the first temperature peak following the transport peak at 130-m depth in Lombok Strait and at 230-m depth in Ombai Strait, linking positive transport anomalies to positive temperatures and negative transport anomalies to negative temperatures. Averaged over all 40 events, the lag between the transport and temperature peaks is 11 ± 9 days in Lombok Strait and 12 ± 12 days in Ombai Strait, consistent with the observation that the relative timing of the transport and temperature signals is highly variable. The value of these lags is the same for both downwelling and upwelling events. In both straits, the peak (absolute) temperature and transport anomalies associated with each Kelvin wave event are significantly correlated, with $R^2 = 0.21$ in Lombok Strait and 0.28 in Ombai Strait (Fig. 9). These results indicate that the strength of Kelvin wave transport anomalies is positively correlated with the strength of Kelvin wave temperature anomalies but that the relative phasing between the transport and temperature is highly variable.

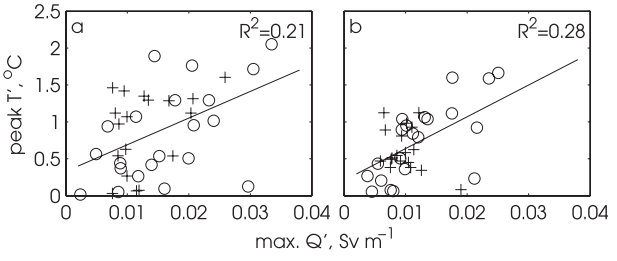

FIG. 9. Scatterplots comparing absolute value of peak transport and temperature anomalies associated with downwelling (circles) and upwelling (pluses) Kelvin wave events at (a) Lombok Strait and (b) Ombai Strait. Note that the peak can refer to positive or negative values. Temperature data are from the instrument closest to the surface in each strait: ~130 m at Lombok Strait and ~230 m at Ombai Strait. Lines and R^2 values are result of linear least-squared regressions. Both are statistically significant (95% significance cutoff is 0.10).

d. Wind forcing

Previous observational and modeling studies (e.g., Qiu et al. 1999) have demonstrated that Indian Ocean winds are the dominant source of intraseasonal energy in the Lombok and Ombai Straits. We thus only consider the Indian Ocean as the primary source of the intraseasonal transport signal in the Lombok and Ombai Straits, although there are doubtless small intraseasonal signals originating locally or in the Pacific Ocean (Schiller et al. 2010).

To place the ITF observations into the larger context of Indian Ocean dynamics, each of the Kelvin wave events was linked to a signal in wind. We used zonal winds averaged over 2°S–2°N in the equatorial Indian Ocean and alongshore winds averaged over a 2°-wide strip along the Sumatra and Java coasts (Fig. 1). The mean and the annual and semiannual harmonics were removed from the winds at each longitude, and the winds were bandpassed with a 20–365-day window. To associate Kelvin waves with wind anomalies, we used the line that was fit to the SLA (Fig. 3a) to extract the wind signal for a 10-day-wide strip preceding each Kelvin wave. We then picked out the peak wind along this strip, assuming that westerly (positive) winds force downwelling Kelvin waves and easterly (negative) winds force upwelling waves, and the nearest ± 2 m s^{-1} contour associated with the peak wind was identified as the event that forced the Kelvin wave. Figure 3b shows the wind field and the contour associated with each Kelvin wave. Having an estimate of the location and magnitude of each wind peak allowed us to quantify the characteristics of the wind forcing in terms of its longitude and strength, and associating each event with a wind contour allowed us to quantify the duration and longitudinal span of the wind bursts. These are somewhat arbitrary metrics for characterizing the wind events, but they allow a comparison of the different events. Typically, wind events are seen to the west of SLA events, as would be expected for winds forcing an eastward-propagating SLA signal. In general, westerly and easterly wind bursts share fairly similar characteristics: westerly events are centered around 80° ± 13°E and easterlies are centered around 78° ± 9°E. Westerlies tend to have a slightly greater fetch, with an average longitudinal span of around 32° and a duration of 20 days, compared with around 27° and 15 days for easterlies. Contrary to previous observations (Waliser et al. 2003; Iskandar et al. 2005), we did not notice strong seasonal asymmetries in the properties of the wind events, and we were thus unable to find a clear connection between the prevalence of mode-2 events in boreal summer and the wind forcing.

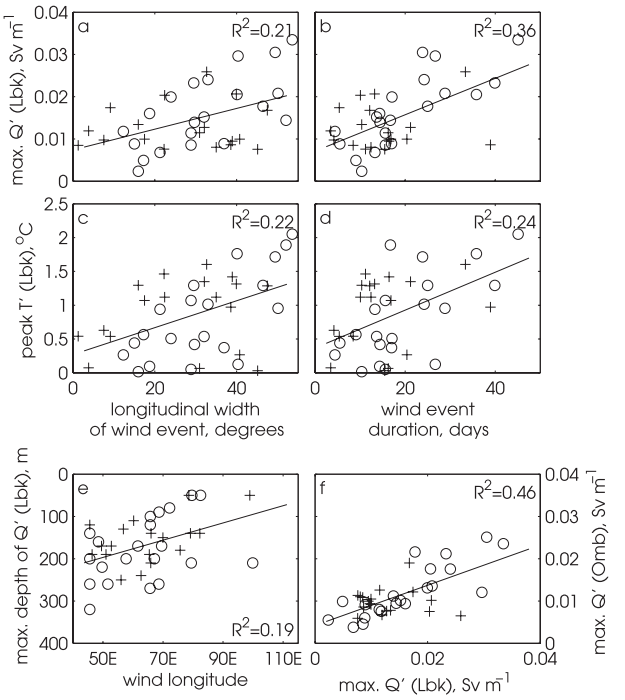

FIG. 10. Scatterplots comparing transport, temperature, and wind properties of downwelling (circles) and upwelling (pluses) Kelvin wave events. Lines and R^2 values are result of linear least square regressions. All are statistically significant (90% significance cutoff is 0.07 and 95% significance cutoff is 0.10): (a) magnitude of peak Lombok Strait transport anomaly due to the Kelvin wave vs longitudinal extent of the wind event; (b) magnitude of peak Lombok Strait transport anomaly vs duration of the wind event; (c) magnitude of peak Kelvin wave temperature anomaly observed in Lombok Strait vs longitudinal extent of the wind event; (d) magnitude of peak Lombok Strait temperature anomaly vs duration of the wind event; (e) depth penetration of transport anomaly in Lombok Strait vs westernmost longitude of wind patch; and (f) magnitude of peak transport anomaly seen in Ombai vs in Lombok Strait.

The exercise of associating each Kelvin wave with an Indian Ocean SLA and wind anomaly and an ITF transport and temperature anomaly allowed us to evaluate how the wind forcing affects the characteristics of the Kelvin waves. This was done using a series of scatterplots comparing the properties of each of the events, including wind strength, location, and duration; peak transport anomaly and depth; total transport anomaly; and peak temperature anomaly (Fig. 10). Generally, Kelvin wave transport anomalies have similar amplitudes in the Lombok and Ombai Straits (Fig. 10f), and Kelvin waves with large transport anomalies also have large temperature anomalies (not shown). The strength of the Kelvin wave transport and temperature anomalies is well correlated with wind fetch: for both downwelling and upwelling Kelvin waves, the amplitude of the transport anomalies had positive correlations with wind

duration and longitudinal extent (Figs. 10a,b). These wind properties are also well correlated with Kelvin wave temperature anomalies (Figs. 10c,d). In agreement with linear ray theory [Eq. (2)], Kelvin waves forced farther west in the basin tend to penetrate deeper in the water column (Fig. 10e).

5. Energy pathways

a. Partitioning of energy at Lombok Strait

Tracking the Kelvin wave signal in SLA is an effective way to evaluate the pathways the waves take as they propagate. Lombok Strait is 35 km wide and the Rossby radius of deformation here is around 100 km, so an oft-asked question is whether Kelvin wave energy enters Lombok Strait and if so how much. Syamsudin et al. (2004) associated annual maxima in altimetric SLA measurements with the single largest Kelvin wave observed each year from 1993 to 2001 and then compared the spectral energy east and west of Lombok Strait. From this technique, they estimated that 56% of incoming Kelvin wave energy enters Lombok Strait, with a standard deviation of 14% over the 9-yr time period. Note, however, that this estimate was based on the semiannual Kelvin wave and therefore is not necessarily directly comparable to the intraseasonal Kelvin waves considered in the present study. Here, we examine the SLA signals of the individual Kelvin waves to identify the pathway of intraseasonal Kelvin waves. For each individual event, we extracted the SLA signal over areas 2° to the west and to the east of Lombok Strait (regions *W* and *E* in Fig. 1). The root-mean-square SLA ($\mathrm{rms_{SLA}}$) in these regions over the course of each event was used as a proxy for Kelvin wave energy, and comparing the $\mathrm{rms_{SLA}}$ values at *W* and *E* gave an estimate of how much of the incoming energy was siphoned north into Lombok Strait. Averaged over the 40 Kelvin waves observed during the INSTANT period, 37% ± 9% of the incoming Kelvin wave energy bypassed Lombok Strait and continued east along the coastal waveguide. This implies that approximately 63% of the incoming energy entered Lombok Strait or was dissipated or reflected off the topography in that region. This ratio is the same within statistical error bars for downwelling and upwelling Kelvin waves, although generally a greater percentage of the incoming energy of downwelling waves enters Lombok Strait compared with upwelling waves. We found no clear relationship between wind strength or fetch and the ratio of $\mathrm{rms_{SLA}}$ east and west of Lombok Strait, indicating that the winds are not the primary determining factor for how much Kelvin wave energy enters Lombok Strait.

b. Kelvin waves north and south of Sumba Island

S09 suggested that, as the Kelvin waves propagate eastward along the Nusa Tenggara waveguide from Lombok to Ombai, there are two pathways that the waves could take (Fig. 1). North of Sumba Island, the sill depth is around 900 m and Kelvin wave energy shallower than this depth likely propagates directly to Ombai Strait, whereas deeper Kelvin wave energy may be blocked by the sill. The deeper waves could conceivably either pass through Savu/Dao Strait (sill depth 1150 m) into the Savu Sea to Ombai Strait or, if deeper than this sill, proceed southward into Timor Passage (S09). For now, we only consider whether the waves propagate north versus south of Sumba Island. For each of the 40 events, we extracted the Kelvin wave SLA along the path north and south of Sumba Island and computed the $\mathrm{rms_{SLA}}$ of the signal over the duration of the event and longitude range of Sumba Island (117°–122°E; shaded regions labeled *N* and *S* in Fig. 1). The ratio of the $\mathrm{rms_{SLA}}$ along the two paths *N*:*S* was then used as an estimate of how much of the incoming energy went north or south of the island. Averaged over all 40 events, *N*:*S* was equal to around 1.0 ± 0.1, meaning that half of the incoming Kelvin wave energy goes north of Sumba Island. Separating the two types of events shows that more of the incoming energy for downwelling Kelvin waves goes south of Sumba Island and more of the upwelling Kelvin wave energy travels north of Sumba Island; for the downwelling events, *N*:*S* was equal to around 0.6 ± 0.2, whereas for the upwelling events the ratio was 1.3 ± 0.2. There is little correlation between the amount of Kelvin wave energy going north versus south of Sumba Island and the depth of the maximum transport anomalies seen in either the Lombok or Ombai Straits. This suggests that the routing of the Kelvin waves north or south of Sumba Island does not necessarily arise from differences in the depth penetration or structure of the Kelvin waves as hypothesized by S09. The *N*:*S* ratio is also not well correlated with wind strength, location, or fetch, and the ratio does not have an obvious seasonal cycle.

6. Wind-forced model

Kelvin wave dynamics in the ITF region can also be explored using a simple wind-forced model in which the ocean is considered to be a linear, continuously stratified fluid, and wind stress is applied as a body force over a shallow mixed layer (cf. Cane 1984; Kessler and McPhaden 1995). The Kelvin wave response is determined by integrating along the characteristic $x - ct =$ constant, from the western edge of the Indian Ocean basin (50°E) to a point x_o along the Kelvin wave path.

Each mode of some modeled quantity A_n (e.g., sea level, velocity, pressure, etc.) is computed individually, then the modes are summed to give the total response. The generalized formulation for this is given by

$$A(x_o, z, t) = \sum_{n=1}^{\infty} \alpha_n(z) \int_{50°\mathrm{E}}^{x_o} \tau^x\left(x, t + \frac{x - x_o}{c_n}\right) dx, \quad (4)$$

where α_n is the coefficient for the mode-n part of the modeled signal, c_n is the baroclinic phase speed, and τ^x is the zonal wind stress. To model A_n as sea level, $\alpha_n = \psi_n(0)^2/\rho g D$, where $\psi_n(0)$ is the vertical structure function $\psi_n(z)$ [Eq. (1)] at the surface ($z = 0$), ρ is seawater density, g is the gravitational constant, and D is the bottom depth. To model zonal current as a function of depth, we set $\alpha_n = \psi_n(0)\psi_n(z)/\rho c_n D$ (Kessler and McPhaden 1995).

We used this model to examine some of the noteworthy features of the observations: the role of wind forcing over different parts of the basin, the relative strength of the different baroclinic modes, and the importance of stratification variability. As the baseline case, we forced the model with 6-hourly wind stress along the Kelvin wave path (Fig. 1): zonal winds along the equator over the longitude range 50°–100°E, averaged over 2°S–2°N, and alongshore winds along the Sumatra and Java coasts from 100° to 115°E. We ran the model for the 2004–06 INSTANT deployment period to compare the modeled output with our observations. All model quantities have been filtered in the same manner as the corresponding observations to facilitate the comparisons. The stratification $N(z)$ was obtained from the Argo gridded temperature and salinity fields (Roemmich and Gilson 2009) averaged over the same area as the wind patch during the same time period, and the phase speeds c_n were computed from Eq. (1) using Argo data (Table 1), again for the same space and time period as the wind patch.

To evaluate the success of the model, we used a linear least squares method to fit the observed Lombok Strait velocity at each time to the first four modes of modeled velocity over depths 100–300 m. Averaged over all times, the first two modes accounted for 48% and 38% of the variance of the time series, respectively, with modes 3 and 4 accounting for less than 13%. Modes higher than $n = 2$ can thus reasonably be neglected for comparisons between model results and observations. Even with only the first two modes included, the model effectively reproduces the propagation of the observed Kelvin waves (Fig. 11). The lines fit to the Kelvin wave signals observed in SLA (Fig. 3a) have been superimposed on the modeled SLA (Fig. 11), showing that all of the Kelvin waves seen in the observed SLA were reproduced by the model. This confirms that our observations are entirely consistent with wind-forced Kelvin waves and also validates the effectiveness of the Kelvin wave selection method used to identify the events in the observations. Comparing the timing of the modeled and observed signals shows that, in some cases, the modeled events are slower than the observed events. This difference may be a result of the model's sensitivity to bottom depth and stratification, which are based on the gridded Argo fields and thus are rather coarse. Alternatively, nonlinear effects (e.g., resulting from wave-mean flow interaction) may cause the Kelvin waves to propagate faster than predicted by the model (McPhaden et al. 1986).

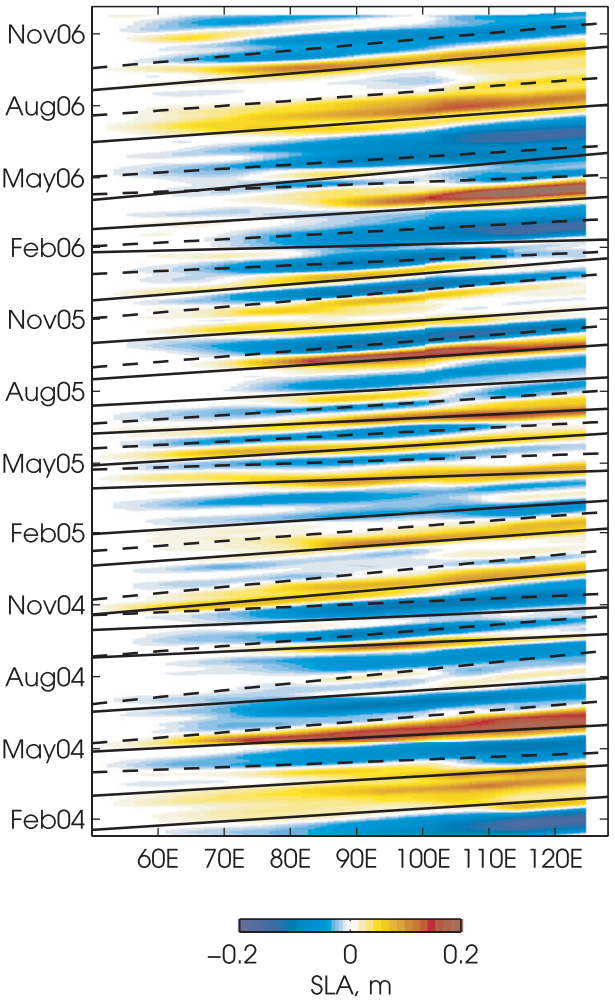

FIG. 11. Model results (sum over first two modes): SLA over the Kelvin wave path. Lines corresponding to paths of the observed downwelling (solid lines) and upwelling (dashed lines) Kelvin waves are shown, as in Fig. 3a.

Figures 12a,b show the observed Lombok Strait transport anomaly and the sum of the first two modes of the modeled transport anomaly, with the times corresponding

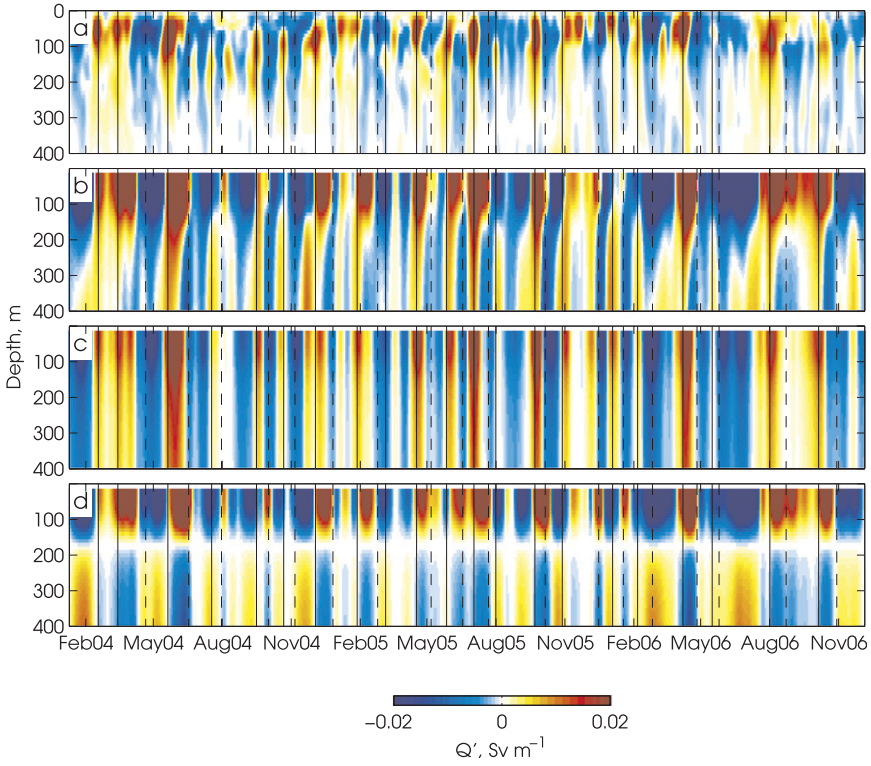

FIG. 12. Intraseasonal transport anomaly in Lombok Strait: (a) observations (as in Fig. 5c), (b) sum over first two modes of the model, (c) modeled mode 1, and (d) modeled mode 2. Vertical lines indicate arrival of observed Kelvin waves, with solid lines denoting downwelling events and dashed lines denoting upwelling events. The thick lines indicate the events with structures that were shown to be dominantly mode 2 in section 4b. The model was forced with winds over 50°–115°E.

to the observed events indicated with vertical lines. The model generally does an excellent job of reproducing the Kelvin wave transports. As is seen in the modeled SLA (Fig. 11), some of the modeled events are slower than the observations by a few days. The mean time difference (Kelvin wave arrival time from model minus observations) is around 4 ± 5 days, where the uncertainty represents the standard deviation over all of the events. Because this time difference is reasonably small and varies over the set of modeled events, it is likely due to small nonlinear effects in the ocean that are not accounted for by the model, for example wave-mean flow interaction. Linear theory requires the superposition of two or more modes for energy to propagate in the vertical. The success of the model in correctly reproducing the observed vertical structure (e.g., the slope of the vertical phase propagation) is dependent on the precise timing of the arrival of the two modes. This is illustrated strikingly when the first- and second-mode responses of the modeled transport anomaly are plotted separately: the first mode is responsible for the dominant signal of the Kelvin wave throughout the water column (Fig. 12c) and the second mode (Fig. 12d) is slower and has a zero crossing at around 180-m depth. Thus, when the modes are added, their relative phasing produces the upward phase propagation characteristic of Kelvin waves. The amplitude of the mode-2 signal is surprisingly large and contributes substantially to the surface signal in Lombok Strait. This has important consequences for understanding and modeling the ITF on intraseasonal time scales: to characterize the surface layer of Lombok Strait, Ekman dynamics alone are not sufficient and remotely forced equatorial waves must be taken into account.

The modeled transport anomaly at Ombai Strait further highlights the importance of the second mode (Fig. 13). As for the modeled Lombok Strait transports, the timing and vertical phase propagation of the Kelvin waves observed in Ombai Strait are well represented by the model. In Lombok Strait, mode 1 more closely resembles the observed transports (Figs. 12a,c), whereas in Ombai Strait the observations throughout the water column look much more like the mode-2 signal (Figs. 13a,d).

The winds used to force the model extend as far east as 115°E. The model does not incorporate any of the effects

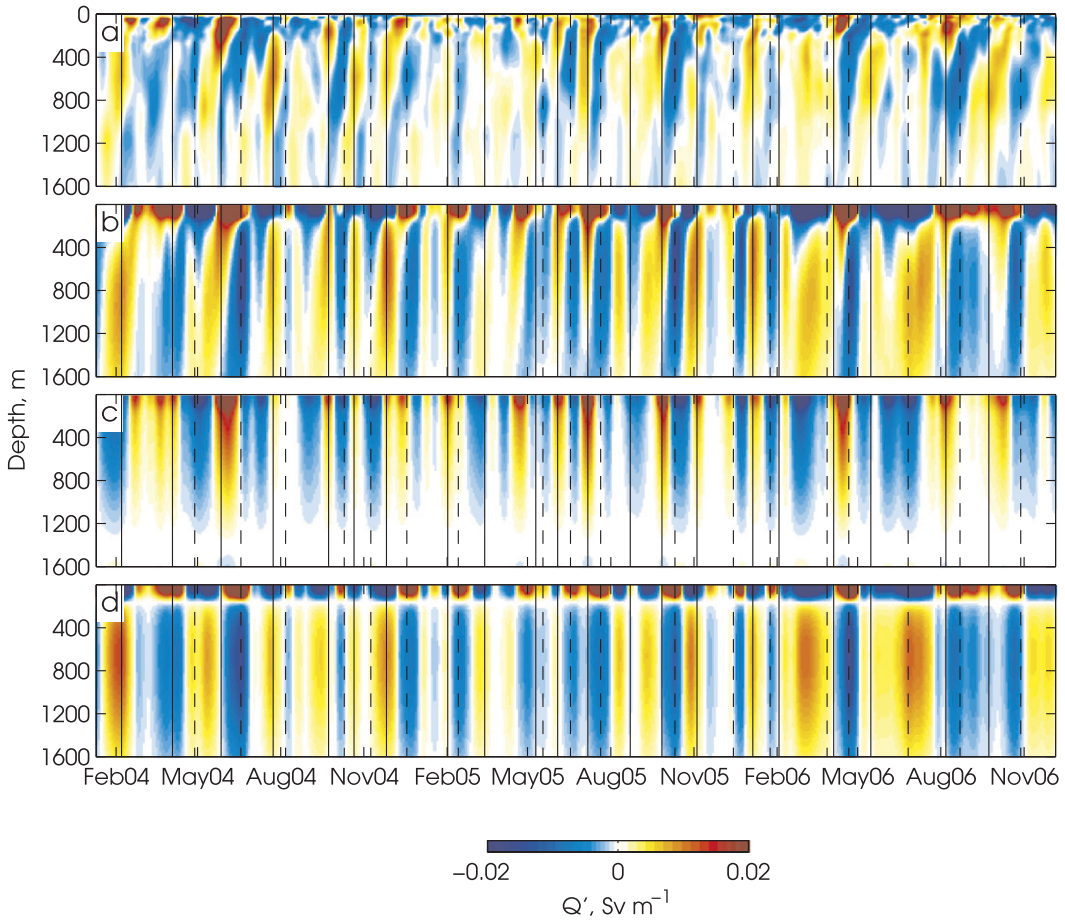

FIG. 13. As in Fig. 12, but for Ombai Strait. Note the different depth scale than in Fig. 12.

of energy dissipation or reflection, and it does not allow any energy to split and go north through Lombok Strait. Stratification does not vary with longitude or time, so the only parameters that change as the waves propagate east of Lombok Strait are the vertical structure functions $\psi(z)$, which vary with bottom depth [Eq. (1)]. It is therefore possible to make a crude estimate of the energy lost to dissipation and reflection, and north through Lombok Strait, by comparing the model output to the observations. In the simplest scenario, a certain percentage α_L of the incoming Kelvin wave energy is siphoned north through Lombok Strait above the 300-m sill. The remaining energy ($1 - \alpha_L$ above the 300-m sill and 100% below it) continues eastward along the waveguide. Downstream of Lombok, the sill will block all of the deep energy below 900- or 1150-m depth, depending on whether the wave travels north or south of Sumba Island. Thus, in this simplistic picture of the dynamics, the Kelvin waves that reach Ombai Strait will be missing α_L of the surface signal and should have zero energy at depth, and the energy at middepth should be a maximum.

The ratio of observed to modeled Kelvin wave transports, calculated at each depth level, should allow us to estimate α_L and assess whether the Kelvin waves go north or south of Sumba Island: that is, over the 900- or 1150-m sill. This ratio is shown in Fig. 14: it was computed by performing a linear regression of the observed versus the modeled transport anomalies at each depth. The error shown in Fig. 14 represents the uncertainty from the regression. As expected, the ratio in the surface layer is low because of the energy that is lost through Lombok Strait. However, instead of being constant above the 300-m Lombok Strait sill depth, the ratio has a minimum (0.06) at the surface and increases to a peak of 0.55 at a depth of around 230 m. This is explained by recalling that the Kelvin waves are diving, so the energy $1 - \alpha_L$ that does not go through Lombok Strait is redistributed vertically as the waves travel eastward. The ratio is fairly constant (0.4–0.5) between around 400 and 800 m; below this depth, the ratio drops off rapidly and falls to zero by 1200 m. Again, the vertical energy propagation can be used to explain why the energy is not zero

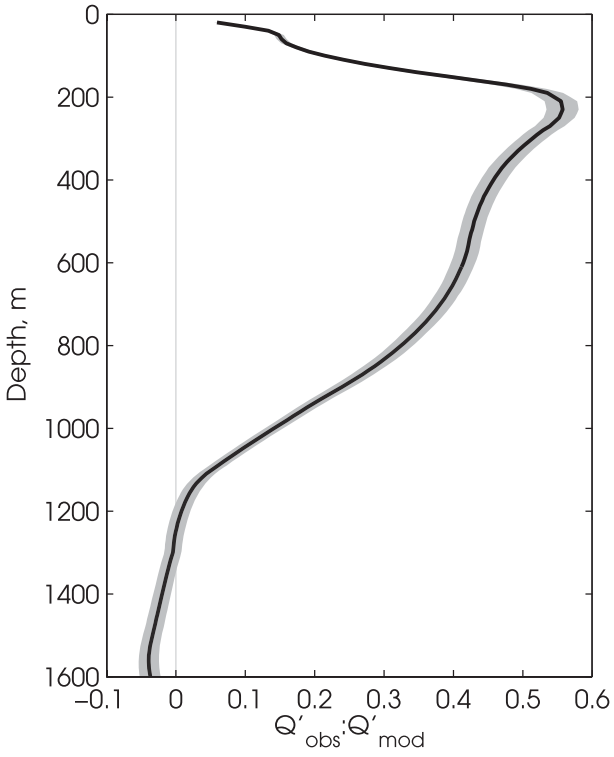

FIG. 14. Ratio of observed to modeled Ombai Strait transport anomaly at each depth. The model was forced with winds over 50°–115°E, and the modeled transport used is the sum over the first two modes.

below the 900–1150-m sill at Sumba Island: some of the Kelvin wave signal at middepths will have been redistributed deeper as the waves dive. There is too much conjecture in this picture of the dynamics to allow us to estimate the energy partitioning at Lombok Strait or to assess whether the deep part of the signal is blocked by the 900-m deep sill at Sumba Strait or the 1150-m deep sill at Savu/Dao Strait. However, the ratio of observed to modeled Kelvin wave transport shown in Fig. 14 is consistent with the expected Kelvin wave dynamics in this region and thus further validates the application of linear ideas to understanding Kelvin wave dynamics in the ITF region.

Figure 15 shows the composited transport anomalies in the Lombok and Ombai Straits using the model output. To form the composites, each of the 21 downwelling and 19 upwelling events observed in the INSTANT data was matched to the corresponding event in the modeled time series by matching peaks in the depth-averaged observed and modeled (mode 1 plus mode 2) Lombok Strait transport data. This gives $t = 0$ for each event, based on the signature of that event in the model. The composites highlight the successes and failures of the model in reproducing the Kelvin waves (Fig. 15). The model correctly shows the strongest transport anomalies at around 100-m depth in Lombok Strait but fails to reproduce the local transport minimum at the surface. At Ombai, the model predicts a strong surface transport anomaly that is not seen in the observations; as discussed above, this is because the model is not able to lose energy into Lombok Strait, so the surface transports are overestimated. The modeled transports penetrate much deeper into the water column than the observed signals, again because of the model's inability to capture the loss of energy resulting from Kelvin waves being blocked by the sills. The modeled Kelvin wave transports persist for roughly 10–14 days, consistent with the observed events. This suggests that the duration and size of the wind events that force the Kelvin waves are linearly related to the duration of the Kelvin waves. Although the model correctly reproduces the upward trend in vertical phase propagation, the slope of this upward phase is not well modeled, as discussed above. In Lombok Strait the vertical propagation of the modeled signal is much more pronounced than in the observations, whereas in Ombai Strait the modeled transport anomalies show virtually no phase propagation between 200- and 1200-m depth. This is not surprising, because neither the mode-1 nor the mode-2 signals vary much over this depth range (Figs. 2, 13).

To test the impact that wind anomalies in different regions have on Kelvin wave generation, we forced the model with winds over a number of different longitude ranges: (i) western equatorial Indian Ocean (50°–75°E); (ii) eastern equatorial Indian Ocean (75°–100°E); (iii) Sumatra and Java coast (100°–115°E); and (iv) along the entire Kelvin wave path (50°–115°E; control case). The results are shown as depth-averaged transports in Fig. 16a. Correlations between the modeled and observed Lombok Strait transports are highest ($R^2 = 0.36$) when winds over the entire Kelvin wave path (control) are used, followed closely by the case of eastern Indian Ocean winds ($R^2 = 0.32$). The amplitude of the signal forced in the control case, winds over the entire Kelvin wave path, is large (standard deviation of 6×10^{-3} Sv m^{-1} compared to the data, which have a standard deviation of 2.6×10^{-3} Sv m^{-1}), whereas the amplitude of the modeled signal forced by only the winds over the eastern Indian Ocean (standard deviation of 3.4×10^{-3} Sv m^{-1}) more closely resembles the data. Interestingly, using just the winds along the Sumatra and Java coasts reproduces the observed Kelvin wave events quite well ($R^2 = 0.17$). The modeled transports forced by winds in the western part of the basin have $R^2 = 0.06$, barely above the 95% significance level of 0.05. These results confirm that the winds in the eastern equatorial Indian Ocean (east of 75°E) dominate the forcing of intraseasonal Kelvin waves,

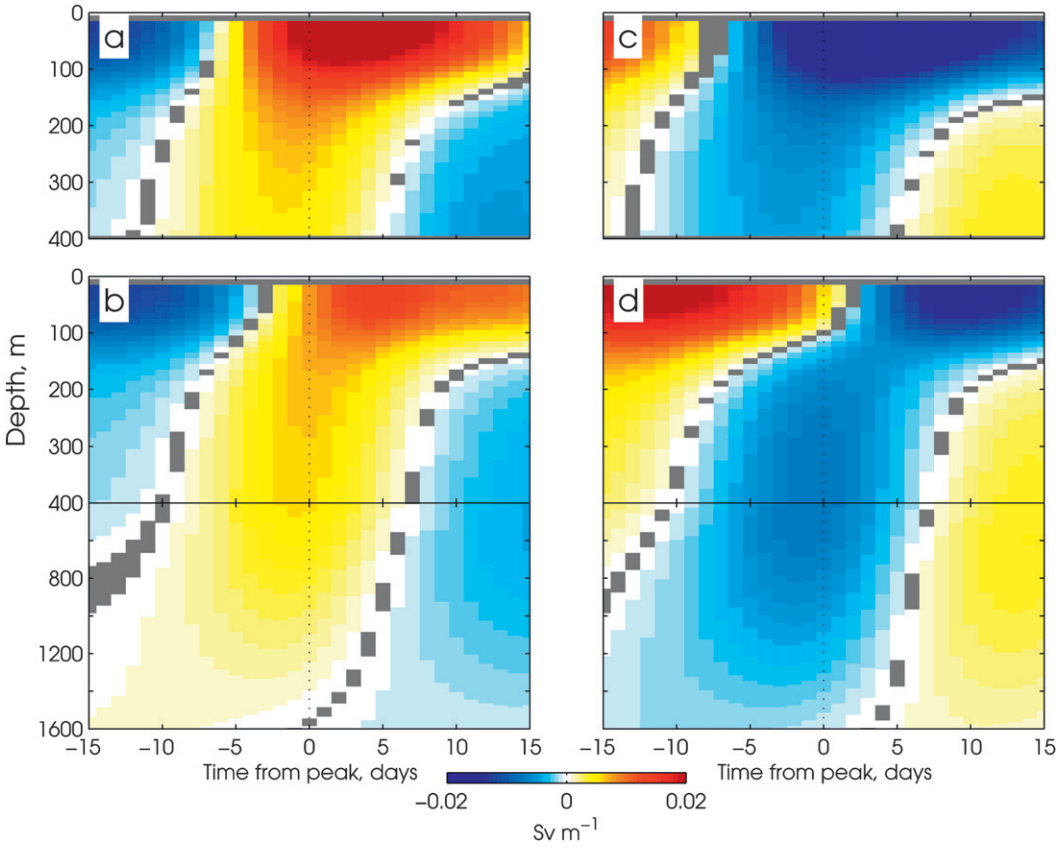

FIG. 15. Composited transport anomalies for downwelling and upwelling Kelvin waves: as in Fig. 6, using the modeled transport anomalies. The model was forced with winds over 50°–115°E, and the output shown is the sum over the first two modes.

but they also highlight the important contribution of the alongshore winds off of Sumatra and Java to the Kelvin wave signal. In a study using European Centre for Medium-Range Weather Forecasts (ECMWF) reanalysis winds, Iskandar et al. (2005) showed that, during boreal summer, intraseasonal variations seen in the ITF region are primarily forced by winds over the eastern Indian Ocean, whereas in boreal winter winds along the Sumatra and Java coasts also contribute significantly. Our results suggest that winds off of Sumatra and Java contribute significantly to the intraseasonal energy in the ITF during all seasons.

Although the linearity assumption implicit in the model requires that $N(z)$ be constant in longitude and time, we explored allowing $N(z)$ to vary on the monthly time and 1° longitude grid of the Argo dataset. The depth-averaged transports that result from using a fixed and a variable Brunt–Väisälä frequency are shown in Fig. 16b. The amplitude of the events is stronger when $N(z)$ is allowed to vary in longitude or time, but neither the timing of the events nor their vertical structures (not shown) are changed, suggesting that seasonal and spatial differences in stratification are not large enough to significantly modify the propagation speeds of either mode-1 or mode-2 Kelvin waves. Because the relative phasing of the two modes determines the vertical structures of the Kelvin waves, seasonal and spatial changes do not appear to be able to account for changes in the vertical structures.

7. Summary

A 3-yr, high-resolution time series of velocities and temperatures was used to observe the vertical structure of Kelvin waves in the ITF outflow passages for the first time. We have identified 40 Kelvin wave events in the Lombok and Ombai Straits associated with transport and temperature anomalies during 2004–06. Each wave was in response to an anomalous Indian Ocean zonal wind event and was associated with an eastward-propagating SLA signal. Consistent with previous observations of equatorial Indian Ocean Kelvin waves, our observations show that westerly wind events produce downwelling Kelvin waves with positive transport anomalies and warm

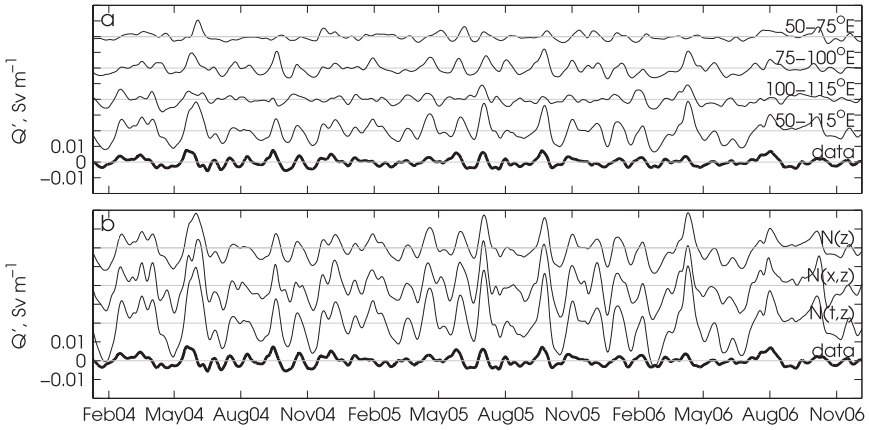

FIG. 16. Sum of first two modes of modeled transport anomalies in Lombok Strait, vertically averaged over depths 100–300 m: (a) using a fixed stratification profile and forced with winds over different longitude ranges along the Kelvin wave path to force the model and (b) forced with winds over the entire Kelvin wave path (50°–115°E) and using a stratification profile that is fixed [$N(z)$], varies with longitude [$N(x, z)$], and varies with time [$N(t, z)$]. In both (a) and (b), the thick line shows the observed vertically averaged Lombok Strait transport anomaly and plots are offset by 0.02 Sv m^{-1}.

temperature anomalies and that easterly wind events produce upwelling Kelvin waves associated with negative transports and cool temperature anomalies. The transport signals observed in the ITF outflow passages are consistent with linear theory and suggest that both upwelling and downwelling Kelvin waves are forced with periodic winds with periods of 28–46 days.

We found correlations between the duration and longitudinal extent of the wind patch that forced each event and the strength of the transport and temperature anomalies in Lombok Strait, consistent with linear model of wind acting as a body force on the surface layer of the ocean and exciting Kelvin waves. Linear ray theory, which is based on the idea that Kelvin waves are a superposition of many baroclinic modes that propagate into the ocean interior as a beam of energy, can also explain the depth of the Kelvin waves observed at Lombok Strait: the farther west a Kelvin wave is generated, the deeper it can penetrate into the water column once it has reached the ITF region. These results suggest that Kelvin waves generally behave in a linear fashion as they propagate through this region.

Altimetric SLA measurements show that 37% ± 9% of the Kelvin wave energy seen just west of Lombok Strait (Fig. 1) bypasses Lombok and continues moving east along the coastal waveguide. The remainder can be assumed to enter the internal seas via Lombok Strait or to be topographically reflected or dissipated. Kelvin wave signals in SLA north and south of Sumba Island indicate that, downstream of Lombok, Sumba Island splits the incoming Kelvin wave energy roughly equally to the north and south.

A linear wind-forced model was used to examine how the behavior and structure of the first two baroclinic modes impacts Kelvin waves observed in the ITF. The model did a good job of reproducing the observations. Comparing the observed and predicted transports at Ombai Strait suggested that a significant portion of the Kelvin wave energy is lost through dissipation and/or reflection off of topography. This comparison also confirmed the basic theory that some of the incoming Kelvin wave signal above 300 m is siphoned north through Lombok Strait and that the deep Kelvin wave signals are blocked by a sill downstream of Lombok Strait. The model showed that the dominant forcing region of intraseasonal Kelvin waves is the equatorial Indian Ocean between 75° and 100°E; the alongshore winds off of Sumatra and Java between 100° and 115°E also contribute significantly to the Kelvin waves observed in the ITF. Wind forcing in the western equatorial Indian Ocean (west of 75°E) contributes little intraseasonal Kelvin wave energy. Finally, we used the model to consider the cases of stratification varying slowly in time or in space: in both cases, the amplitudes of the modeled Kelvin waves are much larger than in the constant stratification case or the data.

Acknowledgments. We thank Sophie Cravatte, whose comments greatly improved this manuscript. The first author gratefully acknowledges assistance from the NASA Earth and Space Science Fellowship. This work was also supported by NSF Grant 0725476. We are grateful to our colleagues Drs. Indroyono Soesilo and Sugiarta Wirasantosa at the Agency for Marine and

Fisheries Research (BRKP), Indonesia, as well as the captains and crews of the *Baruna Jaya I* and *VIII* and the R/V *Southern Surveyor*. The wind data were obtained from Global Modeling and Assimilation Office at the NASA Goddard Space Flight Center, Greenbelt, Maryland. The altimetric SLA products were produced by SSALTO/DUACS and distributed by AVISO with support from CNES.

REFERENCES

Ardizzone, J., R. Atlas, R. Hoffman, J. Jusem, S. Leidner, and D. Moroni, 2009: New multiplatform ocean surface wind product available. *Eos, Trans. Amer. Geophys. Union,* **90,** doi:10.1029/2009EO270003.

Arief, D., and S. Murray, 1996: Low-frequency fluctuations in the Indonesian throughflow through Lombok Strait. *J. Geophys. Res.,* **101** (C5), 12 455–12 464.

Cane, M., 1984: Modeling sea level during El Niño. *J. Phys. Oceanogr.,* **14,** 1864–1874.

Cravatte, S., J. Picaut, and G. Eldin, 2003: Second and first baroclinic Kelvin modes in the equatorial Pacific at intraseasonal timescales. *J. Geophys. Res.,* **108,** 3266, doi:10.1029/2002JC001511.

Drushka, K., J. Sprintall, S. T. Gille, and W. S. Pranowo, 2008: Observations of the 2004 and 2006 Indian Ocean tsunamis from a pressure gauge array in Indonesia. *J. Geophys. Res.,* **113,** C07038, doi:10.1029/2007JC004662.

Ducet, N., P. Y. Le Traon, and G. Reverdin, 2000: Global high-resolution mapping of ocean circulation from TOPEX/Poseidon and ERS-1 and -2. *J. Geophys. Res.,* **105** (C8), 19 477–19 498.

Durland, T., and B. Qiu, 2003: Transmission of subinertial Kelvin waves through a strait. *J. Phys. Oceanogr.,* **33,** 1337–1350.

Eriksen, C., M. Blumenthal, S. Hayes, and P. Ripa, 1983: Wind-generated equatorial Kelvin waves observed across the Pacific Ocean. *J. Phys. Oceanogr.,* **13,** 1622–1640.

Fu, L., 2007: Intraseasonal variability of the equatorial Indian Ocean observed from sea surface height, wind, and temperature data. *J. Phys. Oceanogr.,* **37,** 188–202.

Giese, B. S., and D. E. Harrison, 1990: Aspects of the Kelvin wave response to episodic wind forcing. *J. Geophys. Res.,* **95** (C5), 7289–7312.

Gordon, A. L., R. D. Susanto, A. Ffield, B. A. Huber, W. Pranowo, and S. Wirasantosa, 2008: Makassar Strait throughflow, 2004 to 2006. *Geophys. Res. Lett.,* **35,** L24605, doi:10.1029/2008GL036372.

Han, W., 2005: Origins and dynamics of the 90-day and 30–60-day variations in the equatorial Indian Ocean. *J. Phys. Oceanogr.,* **35,** 708–728.

——, T. Shinoda, L. Fu, and J. McCreary, 2006: Impact of atmospheric intraseasonal oscillations on the Indian Ocean dipole during the 1990s. *J. Phys. Oceanogr.,* **36,** 670–690.

Hautala, S. L., J. Potemra, J. T. Sprintall, J. C. Chong, W. Pandoe, N. Bray, and A. G. Ilahude, 2001: Velocity structure and transport of the Indonesian Throughflow in the major straits restricting flow into the Indian Ocean. *J. Geophys. Res.,* **106** (C9), 19 527–19 546.

Horii, T., H. Hase, I. Ueki, and Y. Masumoto, 2008: Oceanic precondition and evolution of the 2006 Indian Ocean dipole. *Geophys. Res. Lett.,* **35,** L03607, doi:10.1029/2007GL032464.

Iskandar, I., W. Mardiansyah, Y. Masumoto, and T. Yamagata, 2005: Intraseasonal Kelvin waves along the southern coast of Sumatra and Java. *J. Geophys. Res.,* **110,** C04013, doi:10.1029/2004JC002508.

——, Y. Masumoto, and K. Mizuno, 2009: Subsurface equatorial zonal current in the eastern Indian Ocean. *J. Geophys. Res.,* **114,** C06005, doi:10.1029/2008JC005188.

Johnson, E., and M. McPhaden, 1993: Structure of intraseasonal Kelvin waves in the equatorial Pacific Ocean. *J. Phys. Oceanogr.,* **23,** 608–625.

Johnson, H., and C. Garrett, 2006: What fraction of a Kelvin wave incident on a narrow strait is transmitted? *J. Phys. Oceanogr.,* **36,** 945–954.

Kessler, W., and M. McPhaden, 1995: Oceanic equatorial waves and the 1991–93 El Niño. *J. Climate,* **8,** 1757–1774.

Luyten, J., and D. Roemmich, 1982: Equatorial currents at semiannual period in the Indian Ocean. *J. Phys. Oceanogr.,* **12,** 406–413.

Madden, R., and P. Julian, 1971: Detection of a 40–50 day oscillation in the zonal wind in the tropical Pacific. *J. Atmos. Sci.,* **28,** 702–708.

Masumoto, Y., H. Hase, Y. Kuroda, H. Matsuura, and K. Takeuchi, 2005: Intraseasonal variability in the upper layer currents observed in the eastern equatorial Indian Ocean. *Geophys. Res. Lett.,* **32,** L02607, doi:10.1029/2004GL021896.

McCreary, J., 1983: A model of tropical ocean-atmosphere interaction. *Mon. Wea. Rev.,* **111,** 370–387.

——, 1984: Equatorial beams. *J. Mar. Res.,* **42,** 395–430.

McPhaden, M., 2002: Mixed layer temperature balance on intraseasonal timescales in the equatorial Pacific Ocean. *J. Climate,* **15,** 2632–2647.

——, J. Proehl, and L. Rothstein, 1986: The interaction of equatorial Kelvin waves with realistically sheared zonal currents. *J. Phys. Oceanogr.,* **16,** 1499–1515.

Molcard, R., M. Fieux, and F. Syamsudin, 2001: The throughflow within Ombai Strait. *Deep-Sea Res. I,* **48,** 1237–1253.

Peter, B. N., and K. Mizuno, 2000: Annual cycle of steric height in the Indian Ocean estimated from the thermal field. *Deep-Sea Res. I,* **47,** 1351–1368.

Potemra, J., S. Hautala, J. Sprintall, and W. Pandoe, 2002: Interaction between the Indonesian Seas and the Indian Ocean in observations and numerical models. *J. Phys. Oceanogr.,* **32,** 1838–1854.

Qiu, B., M. Mao, and Y. Kashino, 1999: Intraseasonal variability in the Indo-Pacific Throughflow and the regions surrounding the Indonesian Seas. *J. Phys. Oceanogr.,* **29,** 1599–1618.

Qu, T., Y. Du, J. J. P. McCreary, G. Meyers, and T. Yamagata, 2008: Buffering effect and its related ocean dynamics in the Indonesian Throughflow region. *J. Phys. Oceanogr.,* **38,** 503–516.

Rao, S., S. Masson, J. Luo, S. Behera, and T. Yamagata, 2007: Termination of Indian Ocean dipole events in a coupled general circulation model. *J. Climate,* **20,** 3018–3035.

Roemmich, D., and J. Gilson, 2009: The 2004–2008 mean and annual cycle of temperature, salinity, and steric height in the global ocean from the Argo program. *Prog. Oceanogr.,* **82,** 81–100.

Romea, R., and J. Allen, 1983: On vertically propagating coastal Kelvin waves at low latitudes. *J. Phys. Oceanogr.,* **13,** 1241–1254.

Saji, N., B. Goswami, P. Vinayachandran, and T. Yamagata, 1999: A dipole mode in the tropical Indian Ocean. *Nature,* **401,** 360–363.

Schiller, A., S. E. Wijffels, J. Sprintall, R. Molcard, and P. R. Oke, 2010: Pathways of intraseasonal variability in the Indonesian Throughflow region. *Dyn. Atmos. Oceans,* **50,** 174–200, doi:10.1016/j.dynatmoce.2010.02.003.

Schneider, N., 1998: The Indonesian Throughflow and the global climate system. *J. Climate,* **11,** 676–689.

Song, Q., A. Gordon, and M. Visbeck, 2004: Spreading of the Indonesian Throughflow in the Indian Ocean. *J. Phys. Oceanogr.,* **34,** 772–792.

Sprintall, J., J. Chong, F. Syamsudin, W. Morawitz, S. Hautala, N. Bray, and S. Wijffels, 1999: Dynamics of the South Java Current in the Indo-Australian Basin. *Geophys. Res. Lett.,* **26,** 2493–2496.

——, A. Gordon, R. Murtugudde, and R. D. Susanto, 2000: A semiannual Indian Ocean forced Kelvin wave observed in the Indonesian seas in May 1997. *J. Geophys. Res.,* **105** (C7), 17 217–17 230.

——, and Coauthors, 2004: INSTANT: A new international array to measure the Indonesian Throughflow. *Eos, Trans. Amer. Geophys. Union,* **85,** doi:10.1029/2004EO390002.

——, S. E. Wijffels, R. Molcard, and I. Jaya, 2009: Direct estimates of the Indonesian Throughflow entering the Indian Ocean: 2004–2006. *J. Geophys. Res.,* **114,** C07001, doi:10.1029/2008JC005257.

Stammer, D., and C. Wunsch, 1999: Preliminary assessment of the accuracy and precision of TOPEX/POSEIDON altimeter data with respect to the large-scale ocean circulation. *J. Geophys. Res.,* **99** (C12), 24 584–24 604.

Syamsudin, F., A. Kaneko, and D. B. Haidvogel, 2004: Numerical and observational estimates of Indian Ocean Kelvin wave intrusion into Lombok Strait. *Geophys. Res. Lett.,* **31,** L24307, doi:10.1029/2004GL021227.

van Aken, H. M., I. S. Brodjonegoro, and I. Jaya, 2009: The deep-water motion through the Lifamatola Passage and its contribution to the Indonesian throughflow. *Deep-Sea Res. I,* **56,** 1203–1216, doi:10.1016/j.dsr.2009.02.001.

Vinayachandran, P. N., J. Kurian, and C. P. Neema, 2007: Indian Ocean response to anomalous conditions in 2006. *Geophys. Res. Lett.,* **34,** L15602, doi:10.1029/2007GL030194.

Waliser, D. E., R. Murtugudde, and L. E. Lucas, 2003: Indo-Pacific Ocean response to atmospheric intraseasonal variability: 1. Austral summer and the Madden-Julian Oscillation. *J. Geophys. Res.,* **108,** 3160, doi:10.1029/2002JC001620.

Wijffels, S., and G. Meyers, 2004: An intersection of oceanic waveguides: Variability in the Indonesian Throughflow region. *J. Phys. Oceanogr.,* **34,** 1232–1253.

Wyrtki, K., 1973: An equatorial jet in the Indian Ocean. *Science,* **181,** 262–264.

Yu, L., and M. M. Rienecker, 1999: Mechanisms for the Indian Ocean warming during the 1997–98 El Niño. *Geophys. Res. Lett.,* **26,** 735–738.

——, and ——, 2000: Indian Ocean warming of 1997–1998. *J. Geophys. Res.,* **105** (C7), 16 923–16 939.

Zhang, C., 2005: Madden-Julian oscillation. *Rev. Geophys.,* **43,** 1–36.